Recent advances on natural depsidones: sources, biosynthesis, structure-activity relationship, and bioactivities

Maan T. Khayat[1], Kholoud F. Ghazawi[2], Waad A. Samman[3], Aisha A. Alhaddad[3], Gamal A. Mohamed[4] and Sabrin RM Ibrahim[5,6]

[1] Department of Pharmaceutical Chemistry, Faculty of Pharmacy, King Abdulaziz University, Jeddah, Saudi Arabia
[2] Clinical Pharmacy Department, College of Pharmacy, Umm Al-Qura University, Makkah, Saudi Arabia
[3] Department of Pharmacology and Toxicology, College of Pharmacy, Taibah University, Al-Madinah Al-Munawwarah, Saudi Arabia
[4] Department of Natural Products and Alternative Medicine, Faculty of Pharmacy, King Abdulaziz University, Jeddah, Saudi Arabia
[5] Department of Pharmacognosy, Faculty of Pharmacy, Assiut University, Assiut, Egypt
[6] Department of Chemistry, Batterjee Medical College, Jeddah, Saudi Arabia

Corresponding author
Sabrin RM Ibrahim,
sabrin.ibrahim@bmc.edu.sa

ABSTRACT

Depsidones are a class of polyphenolic polyketides that have been proposed to be biosynthesized from oxidative coupling of esters of two polyketidic benzoic acid derivatives. They are principally encountered in fungi and lichens. In addition to their diversified structural features, they revealed varied bioactivities such as antimicrobial, antimalarial, cytotoxic, anti-inflammatory, anti-*Helicobacter pylori*, antimycobacterial, antihypertensive, anti-diarrheal, antidiabetic, phytotoxic, anti-HIV, anti-osteoclastogenic, and butyrylcholinesterase, tyrosinase, hyaluronidase, and acetylcholinesterase inhibition. The current work was targeted to provide an overview on the naturally reported depsidones from various sources in the period from 2018 to the end of 2022 including their structures, biosynthesis, sources, and bioactivities, as well as the reported structure-activity relationship and semisynthetic derivatives. A total of 172 metabolites with 87 references were reviewed. The reported findings unambiguously demonstrated that these derivatives could be promising leads for therapeutic agents. However, further *in-vivo* evaluation of their potential biological properties and mechanistic investigations are needed.

INTRODUCTION

Nature affords unlimited riches of novel biomolecules that are derived from living organisms, including animals, plants, and microorganisms (*Abdel-Razek et al., 2020*). These metabolites have played a fundamental role for thousands of years as remediation for various human illnesses because of their availability and low cost, particularly in developing countries. Also, their chemical diversity with broad bioactivities makes them

invaluable sources of drug development and discovery (*Abdel-Razek et al., 2020*; *Shen, 2015*).

Depsidones are polyphenolic polyketides featuring a tricyclic framework that have a central seven-membered lactone ring; 11H-dibenzo[b,e][1,4]dioxepin-11-one (*Nguyen et al., 2020*; *Sedrpoushan, Haghi & Sohrabi, 2022*). This ring is resulted from ester and ether linkages joining the two ß-orcinol or orcinol-derived rings (*Bay et al., 2020*; *Bai, Yang & Bai, 2021*). Biosynthetically, three to seven carbon chains may be connected at C-1 and C-5 of the rings relying on the starting precursor utilized by PKSs (polyketide synthases) to assemble their backbones (*Singh et al., 2021*). Also, they are proposed to be originated from depsides, which are formed by ester-linking among two orsellinic acid derivatives followed by ether formation (*Ibrahim et al., 2018*, *2021*; *Burt, Harper & Cool, 2022*). Their biosynthesis had been previously discussed in some reports (*Ibrahim et al., 2018*, *2021*; *Singh et al., 2021*). Additionally, ring modifications and side chains constitute the characteristic features of different depsidones (*Jin et al., 2018*; *Mathioudaki et al., 2018*). Some of the reported derivatives possess halogen atoms, like chloride as a substituent on their skeletons (*Duong et al., 2015*). Other reported halogenated derivatives were biosynthesized as a result of modification of the culture media using KBr, NaBr, or porcine. NaBr (*Guo et al., 2022*; *Morshed et al., 2018*; *Sureram et al., 2013*). These metabolites were principally encountered in fungi, lichens, and plants and were rarely reported from marine sources (*Hartati, Megawati & Antika, 2022*; *Sepúlveda et al., 2022*; *Ismed et al., 2021*). Naturally occurring depsidones have been reported to display a span of bioactivities including antimicrobial, antimalarial, cytotoxic, anti-*Trypanosoma*, anti-inflammatory, anti-*Helicobacter pylori*, antimycobacterial, antihypertensive, anti-diarrheal, larvicidal, antidiabetic, herbicidal, antileishmanial, phytotoxic, anti-HIV, anti-osteoclastogenic, and butyrylcholinesterase, aromatase, tyrosinase, hyaluronidase, and acetylcholinesterase inhibition (*Addo et al., 2021*; *Ibrahim et al., 2018*). These compounds have attracted considerable research interest because of their structural diversity and varied bioactivities. This class of metabolites had been reviewed in some previous works. For example, a review by *Ibrahim et al. (2018)* discussed the isolation, structural characterization, biosynthesis, and bioactivities of 84 depsidones reported from fungal sources. Additionally, two published reviews by *Ureña-Vacas et al. (2022)* and *Stojanovic, Stojanovic & Smelcerovic (2012)* focused on lichen depsidones, including their structures and biological activities. Due to the rapid research growing on these metabolites, the current review is an update to the formerly published review in 2018 (*Ibrahim et al., 2018*). In addition, the current work focused on the reported depsidones from various sources in the period from 2018 to the end of 2022 as shown in Fig. 1 and Table S1.

It described a comprehensive summary of the published information on depsidones regarding their sources (fungi, lichens, and plants) (Fig. 2), separation, structural characterization, biosynthesis, semi-synthesis, bioactivities, and structure-activity relation.

This work aimed to provide natural product researchers with comprehensive references that can help them in the identification of separated depsidones from various sources. Additionally, highlighting the reported bioactivities and structure-activity relationship of
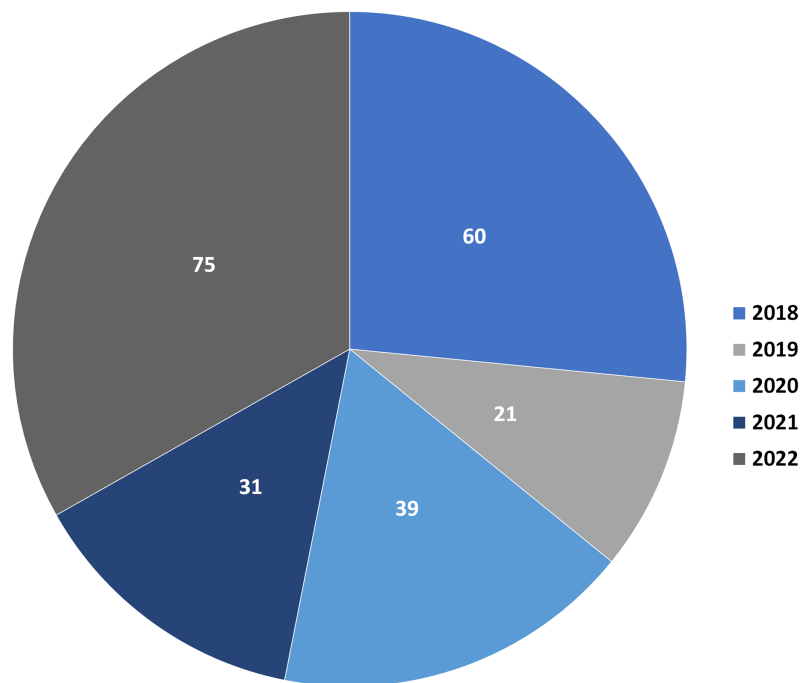
Figure 1 Number of reported depsidones per year in the period from 2018 to 2022.
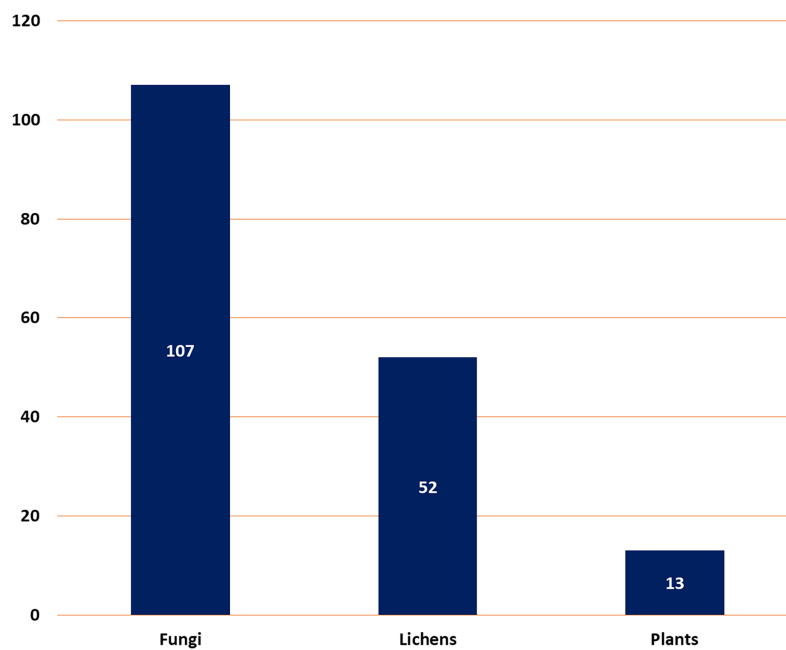
Figure 2 Number of reported depsidones from different sources.
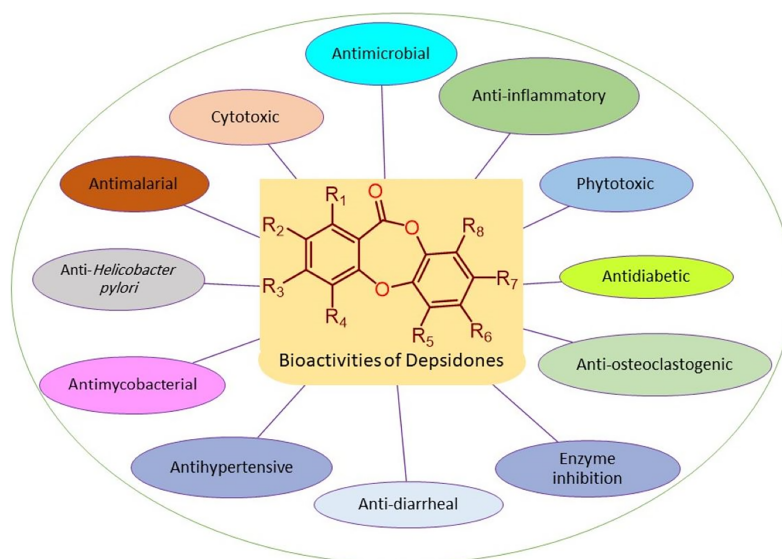
Figure 3 Reported bioactivities of depsidones.

these compounds may draw the interest of medicinal and synthetic chemists for the synthesis and discovery of new agents utilizing known depsidones as start materials.

METHODOLOGY

The published data on depsidones was obtained by searching articles on various databases and Publishers such as Google-Scholar, PubMed, Science Direct, Bentham, Thieme, Springer, Scopus, Taylor/Francis, and Wiley. The search was done utilizing the keywords: "Depsidone + Lichens", OR "Depsidone + Fungi", OR "Depsidone + Plant" OR "Depsidone + Biological activity" OR "Depsidone + Biosynthesis" OR "Depsidone + Semi-synthesis" OR "salazinic acid", "protocetraric acid", "lobaric acid". This work included the English language published articles in peer-reviewed journals in the period from 2018 to the end of 2022. The published articles reported new biological evaluation of metabolites reported before 2018 had been included. A total of 83 articles had been reviewed. The no full access (*e.g.*, conference proceedings), irrelevant, and non-reviewed journals published articles had been excluded. For the non-English articles, the data are extracted from the English abstracts.
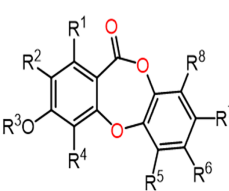
BIOACTIVITIES OF DEPSIDONES

The reported depsidones were assessed for various bioactivities (Figs. 3–13, Tables S2–S6).
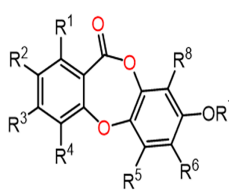
It is noteworthy that some of the reported metabolites had more powerful efficacy than the positive controls. The results of the reported bioactivities were listed and discussed below.

Antimicrobial activity

Currently, antibiotic resistance of microbes has become one of the utmost serious menaces to human health (*Fjell et al., 2012*). The global amplification and rapid growth of multi-resistant microbes that are untreatable with the current antimicrobial therapy have

Compound	R1	R2	R3	R4	R5	R6	R7	R8
Polyanthadepsidone A (1)	OH	CH₃	CH₃	OH	CH₃	OH	CH₃	CH₃
Cetraric acid (2)	CH₃	H	H	CHO	CH₃	COOH	OCH₃	CH₂OCH₂CH₃
Psoromic acid (3)	CH₃	H	H	CHO	COOH	H	OCH₃	CH₃
Methyl psoromate (4)	CH₃	H	H	CHO	COOCH₃	H	OCH₃	CH₃
Virensic acid (5)	CH₃	H	H	CHO	CH₃	H	OH	CH₃

Compound	R1	R2	R3	R4	R5	R6	R7	R8
Cordidepsine (6)	CH₃	H	OH	CHO	OH	CH₃	CH₃	H
Corynesidone A (7)	H	OH	H	CH₃	H	OH	H	CH₃
Corynesidone D (8)	CH₃	H	OH	H	CH₃	COOH	H	H
Hypoprotocetraric acid (9)	CH₃	H	OH	CH₃	CH₃	COOH	H	CH₃
Conhypoprotocetraric acid (10)	CH₃	H	OH	CH₃	CH₃	COOH	H	CH₂OH
Gangaleoidin (11)	CH₃	Cl	OH	Cl	CH₃	COOCH₃	CH₃	H
Dioxepin-11-one (12)	CH₃	H	OH	CH₃	CH₃	H	H	CH₃

Figure 4 Chemical structures of depsidone (1–12).
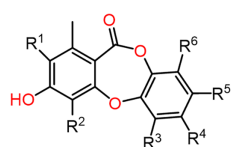
Compound	R1	R2	R3	R4	R5	R6
Parmosidone A (13)	H	CHO	CH₂OH	OH	COOH	CH₃
Parmosidone B (14)	H	OH	CH₂OH	OH	COOH	CH₃
Parmosidone E (15)	H	CHO	CH₃	OH	COOH	CH₃
Vicanicin (16)	Cl	CH₃	CH₃	Cl	OCH₃	CH₃
Protocetraric acid (17)	H	CHO	CH₃	COOH	OH	CH₂OH
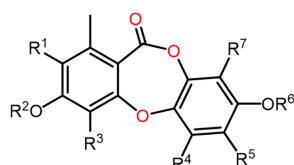
Compound	R1	R2	R3	R4	R5	R6	R7
1H-Dibenzo[b,e][1,4]dioxepin-11-one,3,8-dihydroxy-4-(methoxymethyl)-1,6-dimethyl (18)	H	H	CH₂OH	CH₃	H	H	H
Flavicansone (19)	Cl	CH₃	H	CH₃	Cl	CH₃	CH₃
Baillonic acid (20)	H	CH₃	H	COOH	COOH	CH₃	H
Botryorhodine A (21)	H	H	CHO	CH₃	H	H	H
Botryorhodine B (22)	H	H	CH₃	CH₃	H	H	CH₃
Botryorhodine C (23)	H	H	CH₂OH	CH₃	H	H	CH₃
Botryorhodine D (24)	H	H	CH₂OH	CH₃	H	H	H
Botryorhodine G (25)	H	H	CH₂OCH₃	CH₃	H	H	H
Botryorhodine I (26)	H	H	CH₂OH	CH₃	H	H	OH
Simplicildone A (27)	H	H	CH₂OCH₃	CH₃	H	H	CH₃
Simplicildone B (28)	H	H	CH₂OCH₂CH₃	CH₃	H	H	CH₃

Figure 5 Chemical structures of depsidone (13–28).

been associated with growing morbidity and mortality rates (*Dhingra et al., 2020*). Despite, immense knowledge of this universal health dilemma, developing new-generation antibiotics that combat these microbes has been proven to represent a significant defy (*Bahar & Ren, 2013*). In this regard, many natural metabolites have gained much attention from scientific and pharmaceutical communities because of their antibiotic potential (*Khameneh et al., 2019*). The majority of reported depsidones were assessed for their capacities on various pathogens including antitubercular, anti-phytopathogenic,
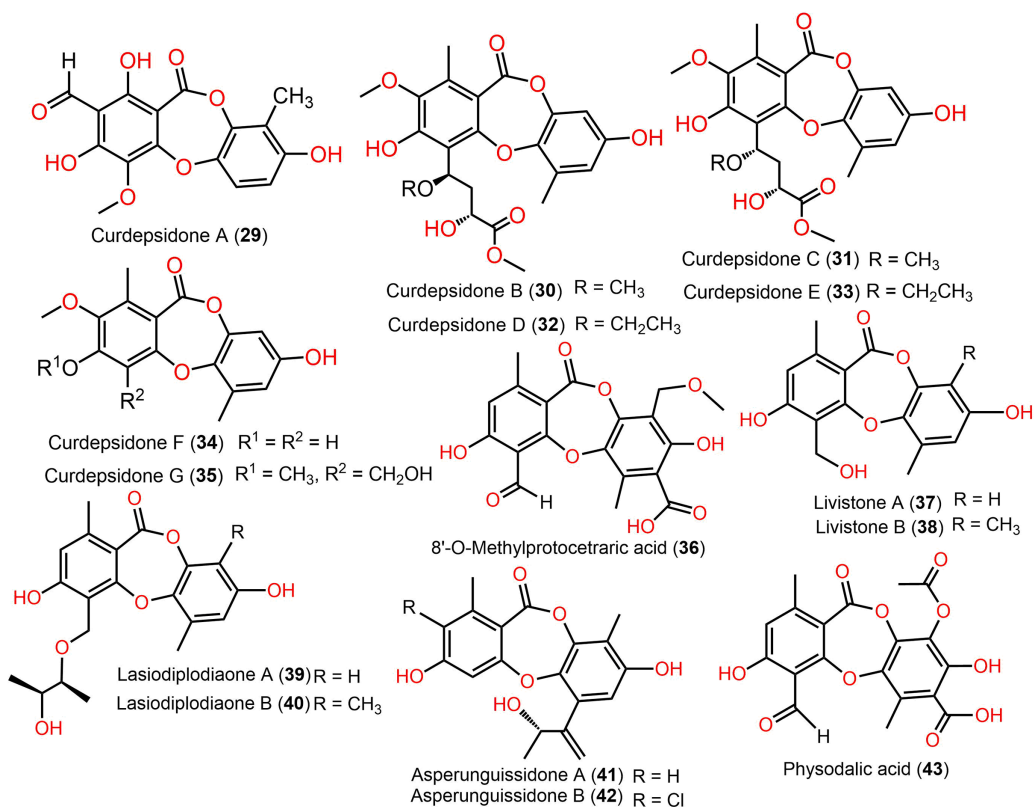
Figure 6 Chemical structures of depsidone (29–43).
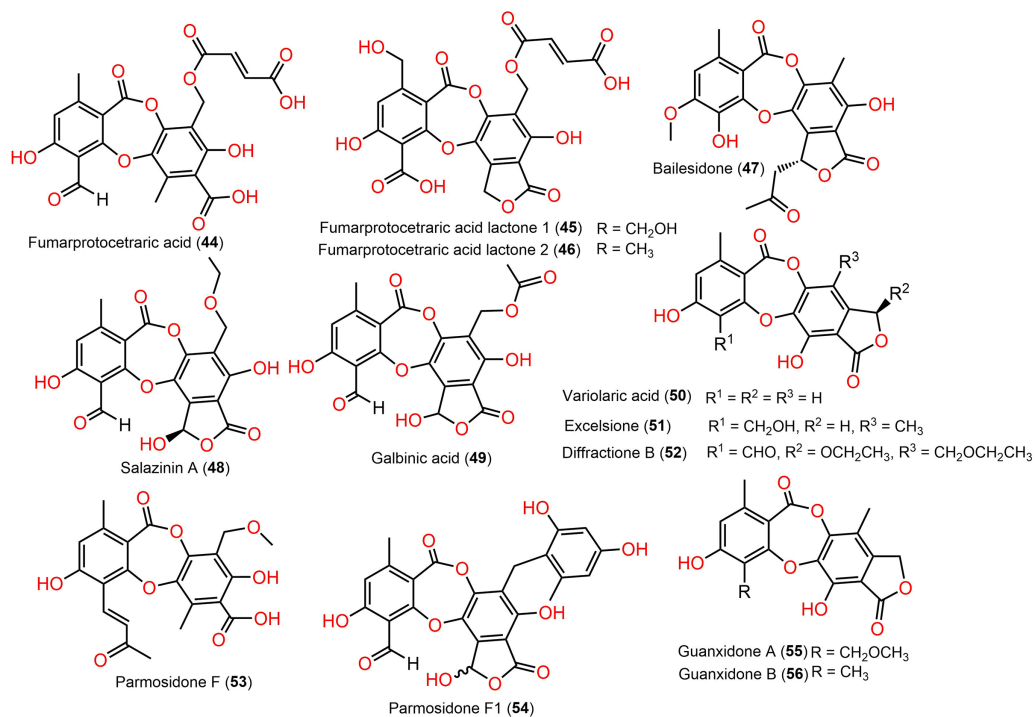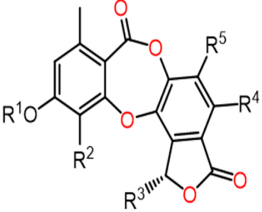
Figure 7 Chemical structures of depsidone (44–56).

Compound	R1	R2	R3	R4	R5
Connorstictic acid (57)	H	CH$_2$OH	CH$_3$	H	CH$_3$
Ceratinalone (58)	CH$_3$	OH	OCH$_2$CH$_3$	OH	CH$_3$
Stictic acid (59)	CH$_3$	CHO	OH	OH	CH$_3$
Norstictic acid (60)	H	CHO	OH	OH	CH$_3$
8`-O-Methylstictic acid (61)	CH$_3$	CHO	OCH$_3$	OH	CH$_3$
8`-O-Ethylstictic acid (62)	CH$_3$	CHO	OCH$_2$CH$_3$	OH	CH$_3$
Neotricone (63)	H	COOH	H	OH	CH$_3$
Conneotricone (64)	H	COOH	H	OH	CH$_2$OH
Salazinic acid (65)	H	CHO	OH	OH	CH$_2$OH
Perisalazinic acid (66)	H	COOH	OH	OH	CH$_2$OH
8'-O-Methylsalazinic acid (67)	H	CHO	OH	OH	CH$_2$OCH$_3$
Norperistictic acid (68)	H	COOH	OH	OH	CH$_3$
Menegazziaic acid (69)	H	CH$_2$OH	OH	OH	CH$_3$
1-Hydroxy-11-(hydroxymethyl)-4,10-dimethoxy-5,8-dimethyl-7H-benzo[6,7][1,4]dioxepino[2,3-e]isobenzofuran-3,7(1H)-dione (70)	CH$_3$	CH$_2$OH	OH	OCH$_3$	CH$_3$
3`-O-Demethylcryptostictinolide (71)	CH$_3$	CH$_2$OH	H	OH	H
Cryptostictic acid (72)	CH$_3$	CH$_2$OH	OH	OH	CH$_3$
Peristictic acid (73)	CH$_3$	COOH	OH	OH	CH$_3$

Figure 8 Chemical structures of depsidone (57–73).

antimalarial, and antibacterial activities. In many studies, they possessed a broad range of activity.

Two new derivatives, simplicildones J (**89**) and K (**90**) and related known compounds **21**, **22**, **27**, and **28** were obtained and characterized from *Simplicillium lanosoniveum* PSUH168 and PSUH261 associated with *Hevea brasiliensis* leaves. Compounds **22** and **27** demonstrated notable antibacterial effectiveness against *Staphylococcus aureus* and MRSA (Methicillin-resistant *S. aureus*, MICs 32.0 µg/mL), while **90** was 4-fold less active compared to vancomycin (MIC 0.5 µg/mL), whilst **90** had (MIC 32 µg/mL) antifungal influence against *Cryptococcus neoformans* ATCC90113 in comparison to amphotericin B (MIC 0.5 µg/mL) (*Rukachaisirikul et al., 2019*).

From *Eucalyptus exserta*-associated *Chaetomium* sp. Eef-10 cultures, new depsidones, mollicellins O–R (**101–104**), in addition to known mollicellins **96–98** were purified using SiO$_2$, Sephadex LH-20, and HPLC and elucidated by spectral analyses. Among these metabolites, **97** (IC$_{50}$s 5.14 and 6.21 µg/mL, respectively) had notable antibacterial capacity against *S. aureus* (ATCC-29213) and *S. aureus* (N50, MRSA) compared to streptomycin sulfate (IC$_{50}$ 1.05 µg/mL for *S. aureus* ATCC-29213) in the broth dilution assay (Table S2) (*Ouyang et al., 2018*).

New members of mollicellin family; mollicellins **108–111**, together with **92**, **94**, **95**, **97**, **99**, **100**, and **104** were separated utilizing SiO$_2$ CC/preparative TLC from Thai rice-accompanied *C. Brasiliense* (*Promgool et al., 2022*). Compounds **92–95**, **108**, and **109** had powerful antibacterial potential against *Bacillus subtilis* and *Bacillus cereus* (MICs 2.0–8.0 µg/mL) which was close to kanamycin (MICs 2.0 µg/mL), however, they displayed moderate efficacy on *S. aureus* ATCC25923 (MICs 16.0–64.0 µg/mL). Besides, **91**, **92**, **97**,
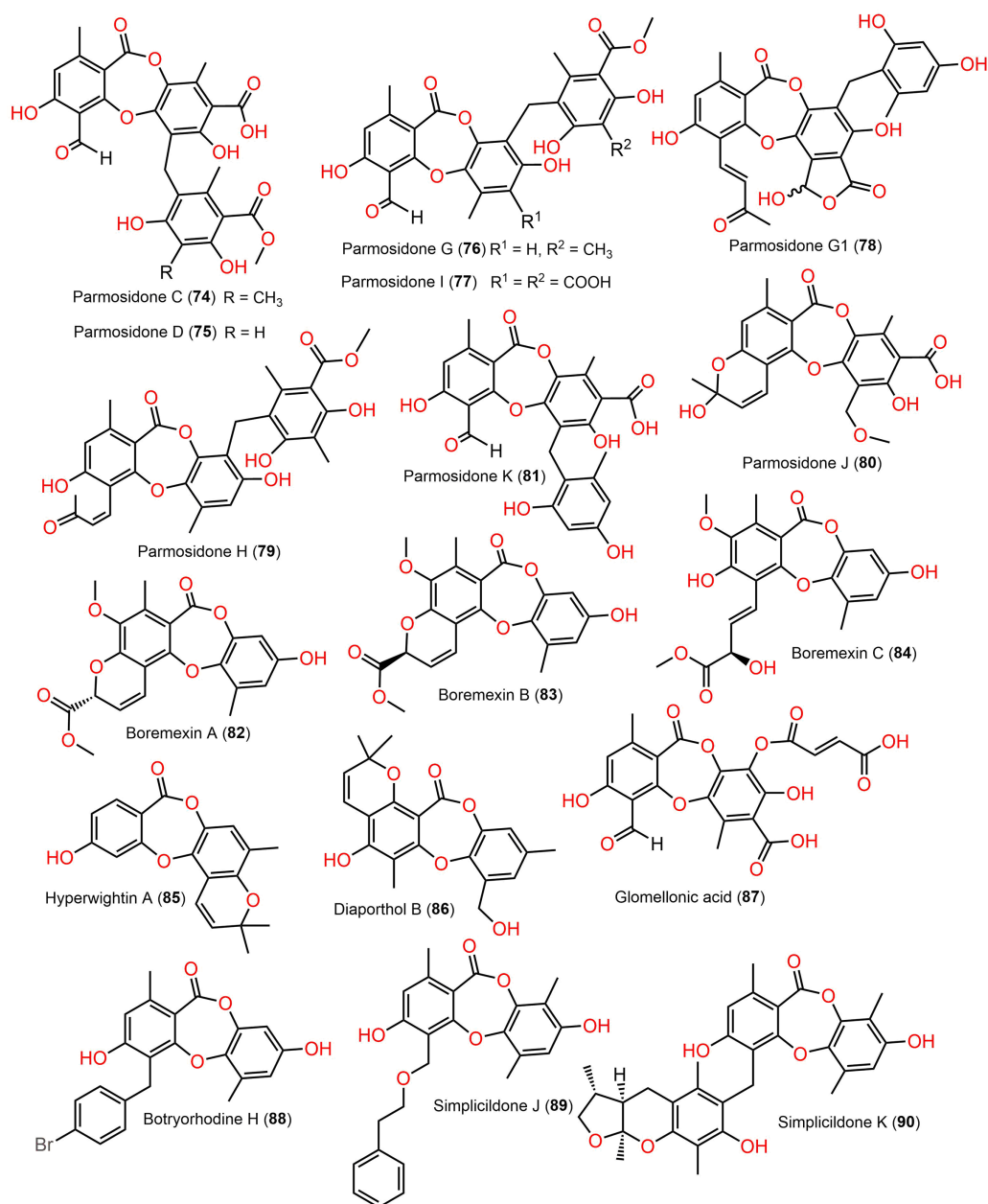
Figure 9 Chemical structures of depsidone (74–90).

110, and **111** were moderately active against different MRSA isolates (ATCC33591, ATCC33592, and ATCC43300, MICs 32.0–128.0 µg/mL) with the same MICs as oxacillin (MICs 32.0–128.0 µg/mL), whereas **91** and **92** also had moderate influence (MICs 32.0–128.0 µg/mL) against *S. aureus* SA1-3 clinical isolates (*Promgool et al., 2022*). It was noted that C-4-CHO and complete lactone ring were significant for antibacterial potential against Gram-positive bacteria (*Promgool et al., 2022*).

Further, new members of mollicellins: **105–107**, and the known mollicellins **93** and **97** were purified from *C. brasiliense* SD-596 rice media utilizing SiO$_2$ CC/HPLC and

Compound	R
Mollicellin B (**91**)	H
Mollicellin M (**99**)	Cl

Compound	R1	R2	R3
Mollicellin C (**92**)	H	CHO	OH
Mollicellin E (**94**)	Cl	CHO	OH
Mollicellin Y (**111**)	H	CH₂OH	CH₃

Compound	R1	R2	R3
Mollicellin D (**93**)	Cl	CH₂OH	H
Mollicellin H (**97**)	H	CHO	H
Mollicellin I (**98**)	H	CH₂OH	H
Mollicellin O (**101**)	H	CH₂OCH₂CH₃	H
Mollicellin S (**105**)	Cl	CHO	CH₃
Mollicellin T (**106**)	Cl	CH₂OH	CH₃
Mollicellin U (**107**)	H	H	H

Compound	R
Mollicellin F (**95**)	Cl
Mollicellin N (**100**)	H

Mollicellin G (**96**)

Mollicellin V (**108**)

Compound	R
Mollicellin P (**102**)	Cl
Mollicellin Q (**103**)	H

Mollicellin R (**104**)

Compound	R
Mollicellin W (**109**)	H
Mollicellin X (**110**)	Cl

Figure 10 Chemical structures of depsidone (91–111).

Compound	R
Auranticin A (**112**)	CH₂OH
Auranticin B (**113**)	CHO
Pilobolusone C (**114**)	CH₂OCH₃

Compound	R1	R2	R3	R4	R5
Spiromastixone A (**115**)	H	H	H	H	H
Spiromastixone B (**116**)	Cl	H	H	H	H
Spiromastixone E (**117**)	Cl	Cl	H	H	H
Spiromastixone F (**118**)	Cl	Cl	Cl	H	H
Spiromastixone G (**119**)	Cl	Cl	Cl	CH₃	H
Spiromastixone I (**120**)	Cl	Cl	Cl	H	Cl
Spiromastixone P (**121**)	H	H	Br	H	H
Spiromastixone P1 (**122**)	H	H	Cl	H	H
Spiromastixone Q (**123**)	H	H	H	H	Br
Spiromastixone Q1 (**124**)	H	H	H	H	Cl
Spiromastixone R (**125**)	H	Br	H	H	Br
Spiromastixone R1 (**126**)	Cl	H	Cl	H	Cl
Spiromastixone S (**127**)	Br	Br	H	H	H
Spiromastixone S1 (**128**)	H	H	COOH	H	H
Spiromastixone T (**129**)	Br	Br	Br	CH₃	Br

Compound	R1	R2	R3	R4	R5
Himantormione A (**130**)	H	(CH₂)₄ CH₃	H	H	(CH₂)₂CH₃
Himantormione B (**131**)	H	(CH₂)₄ CH₃	H	H	(CH₂)₄ CH₃
Norcolensoic acid (**132**)	COOH	(CH₂)₄ CH₃	H	H	(CH₂)₄ CH₃
Norlobaridone (**133**)	H	(CH₂)₄ CH₃	H	H	CH₂ CO(CH₂)₄ CH₃
Physodic acid (**134**)	COOH	(CH₂)₄ CH₃	H	H	CH₂ CO(CH₂)₄ CH₃
3-Hydroxyphysodic acid (**135**)	COOH	(CH₂)₄ CH₃	OH	H	CH₂ CO(CH₂)₄ CH₃
Lobaric acid (**136**)	COOH	(CH₂)₄ CH₃	H	CH₃	CH₂ CO(CH₂)₄ CH₃
Oxolobaric acid (**137**)	COOH	(CH₂)₄ CH₃	H	CH₃	CO(CH₂)₂ COCH₃

Figure 11 Chemical structures of depsidone (112–137).

elucidated by spectral analyses (*Zhao et al., 2021b*). The analogs **97** and **105–107** possessed specific inhibition capacities towards *S. aureus* and MRSA, whereas **105** was the most efficient (MICs 6.25 µg/mL) compared to vancomycin (MICs 1.0 µg/mL); however, they had no efficacy against *Candida albicans* and *Pseudomonas aeruginosa* in the broth microdilution assay. It was noted that substituting 6-OH (in **93**) with OCH₃ (in **106**) and 4-CH₂OH (in **106**) with 4-CHO (in **105**) enhanced the antibacterial capacity. It is worth noting that CHO at C4 and OCH₃ at C7 in **105** could have synergetic efficacy in boosting the antibacterial potential (*Zhao et al., 2021b*). *Zhao et al. (2021b)* postulated the
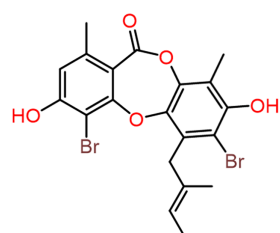
Aspergillusidone F (**153**)
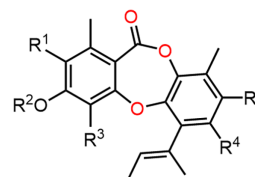
Compound	R1	R2	R3	R4	R5
Unguinol (**138**)	H	H	H	H	H
2-Chlorounguinol (**139**)	Cl	H	H	H	H
2,4-Dichlorounguinol (**140**)	Cl	H	Cl	H	H
2,7-Dichlorounguinol (**141**)	Cl	H	CH₃	Cl	H
4,7-Dichlorounguinol (**142**)	H	H	Cl	Cl	H
3,1`-Dichlorounguinol (**143**)	Cl	H	H	Cl	H
2-Chloro-7-bromounguinol (**144**)	Cl	H	H	Br	H
7-Bromounguinol (**145**)	H	H	H	Br	H
Nidulin (**146**)	Cl	H	Cl	Cl	CH₃
Nornidulin (**147**)	Cl	H	Cl	Cl	H
Aspergillusidone A (**148**)	H	H	H	COOH	OH
Aspergillusidone B (**149**)	H	CH₃	Cl	Cl	OH
Aspergillusidone C (**150**)	Cl	H	H	Cl	OH
Aspergillusidone D (**151**)	Br	H	H	Br	OH
Aspergillusidone E (**152**)	Br	H	H	H	OH
Aspergillusidone H (**154**)	H	CH₃	CH₃	Cl	OH
Aspersidone (**155**)	Cl	H	H	Cl	OCH₃
Aspersidone B (**156**)	Cl	H	H	H	OCH₃

Figure 12 Chemical structures of depsidone (138–156).
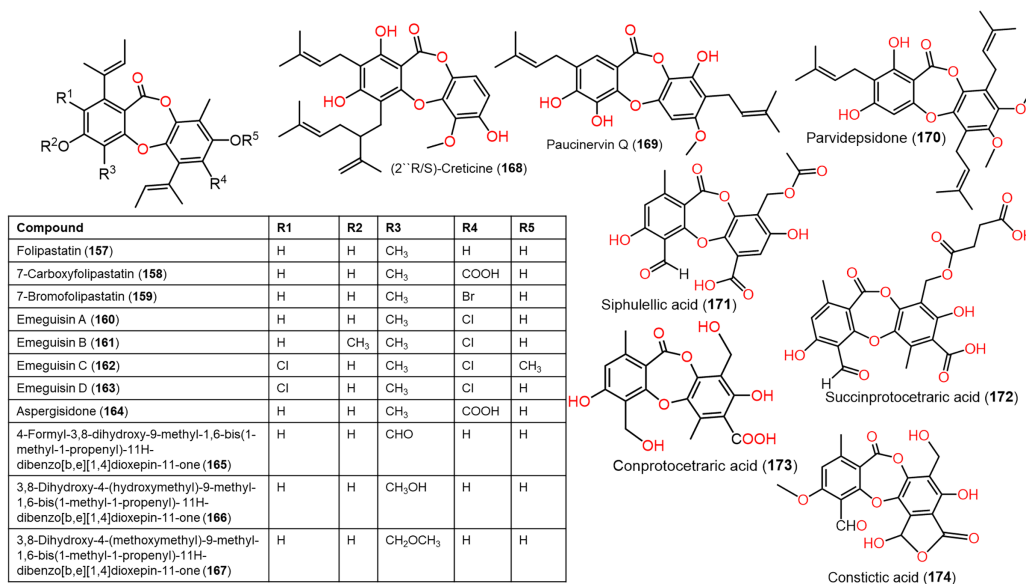
Compound	R1	R2	R3	R4	R5
Folipastatin (**157**)	H	H	CH₃	H	H
7-Carboxyfolipastatin (**158**)	H	H	CH₃	COOH	H
7-Bromofolipastatin (**159**)	H	H	CH₃	Br	H
Emeguisin A (**160**)	H	H	CH₃	Cl	H
Emeguisin B (**161**)	H	CH₃	CH₃	Cl	H
Emeguisin C (**162**)	Cl	H	CH₃	Cl	CH₃
Emeguisin D (**163**)	Cl	H	CH₃	Cl	H
Aspergisidone (**164**)	H	H	CH₃	COOH	H
4-Formyl-3,8-dihydroxy-9-methyl-1,6-bis(1-methyl-1-propenyl)-11H-dibenzo[b,e][1,4]dioxepin-11-one (**165**)	H	H	CHO	H	H
3,8-Dihydroxy-4-(hydroxymethyl)-9-methyl-1,6-bis(1-methyl-1-propenyl)- 11H-dibenzo[b,e][1,4]dioxepin-11-one (**166**)	H	H	CH₃OH	H	H
3,8-Dihydroxy-4-(methoxymethyl)-9-methyl-1,6-bis(1-methyl-1-propenyl)-11H-dibenzo[b,e][1,4]dioxepin-11-one (**167**)	H	H	CH₂OCH₃	H	H

(2``R/S)-Creticine (**168**)

Paucinervin Q (**169**)

Parvidepsidone (**170**)

Siphulellic acid (**171**)

Succinprotocetraric acid (**172**)

Conprotocetraric acid (**173**)

Constictic acid (**174**)

Figure 13 Chemical structures of depsidone (157–174).
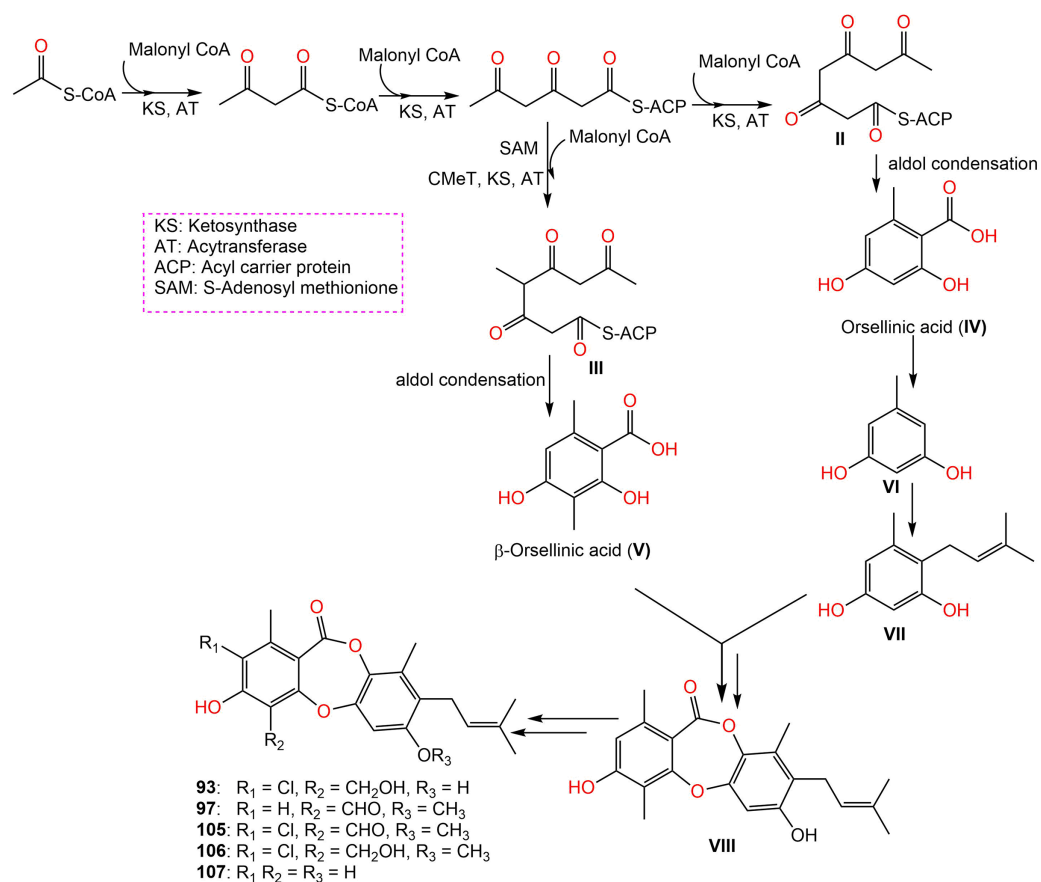
Scheme 1 Biosynthetic pathway of 93, 97, and 105–107 (*Zhao et al., 2021a*, *2021b*).

biosynthetic pathway of these mollicellins as shown in Scheme 1. First, the precursors **II** and **III** were biosynthesized by KS (β-ketoacyl synthase) domain, AT (acyltransferase) domain, ACP (acyl-carrier-protein) domain, and Claisen-type/cyclase-thioesterase domain, in addition to CMeT (C-methyltransferase) domain and SAM (S-adenosyl-methionine) only for **III**. The non-enzymatic aldol condensation of **II** and **III** results in orsellinic acid (**IV**) and β-orsellinic acid (**V**). Decarboxylation of **IV** followed by isoprenylation that are catalyzed by decarboxylase and aromatic prenyl transferase, respectively form **VII**. By oxidase and/or esterase **V** and **VII** are connected to produce **VIII**. Enzymatic oxidation, methylation, or halogenation of **VIII** yield compounds **93**, **97**, and **105–107** (*Zhao et al., 2021a*) (Scheme 1).

From the deep sea-derived *Spiromastix* MCCC3A00308, **122**, **124**, **126**, and **128** were separated and characterized using Sephadex LH-20/HPLC and spectroscopic data, respectively (*Niu et al., 2021a*). Compounds **122**, **124**, **126**, and **128** revealed promising antibacterial influence on *S. aureus* ATCC25923, *Bacillus thuringiensis* ATCC10792, and *B. subtilis* CMCC63501 (MIC ranging from 0.5–32 μg/mL) compared to chloramphenicol (MIC 1.0 μg/mL), while they were weakly active against *E. coli* in the broth microdilution assay. It was found that the tri-chlorinated derivative, **126** (MICs ranged from 0.5 to 1.0

µg/mL) was more powerful than di-chlorinated analog **124**, whereas the latter had more potential than **122** (*Niu et al., 2021a*). Guo et al. separated from ant (*Monomorium chinensis*)-associated *Spiromastix* sp. MY-1 cultivated on KBr-supplemented medium, new brominated derivatives; **121**, **123**, **125**, **127**, and **129** and the known depsidones **115–120** by SiO$_2$ CC/HPLC. These metabolites except **116** and **123** displayed potent growth inhibitory effectiveness (MICs ranged from 5.2–27.6 µM) against plant pathogens; *Xanthomonas oryzae* pv. *oryzae* (Xoo, B1 and B2 strains), *Erwinia amylovora* (B3), *Pseudomonas syringae* pv. *lachrymans* (B4), and *Clavibacter michiganense* subsp. *sepedonicus* (B5), whereas **127** had the strongest potential against *X. oryzae* pv. *oryzae* (MIC 5.2 µM) compared to kanamycin (MICs ranged from 0.54–4.3 µM). *X. oryzae* pv. *oryzae* causes bacterial blight, which is a worldwide devastating rice disease, leading to up to 60% annual yield loss in Asia, it represents one of the utmost fatal rice diseases (*Guo et al., 2022*; *Xu et al., 2015*). Mutualistic microbes with ants were reported as effective protection against plant pathogens and herbivores (*González-Teuber, Kaltenpoth & Boland, 2014*; *Guo et al., 2022*). These findings revealed that **127** could be a potential lead for bactericides to control rice bacterial-blight disease and the ant-accompanied fungi might be a prominent source of bactericide against rice pathogens in the rice system (*Guo et al., 2022*). It is noteworthy that compounds **123**, **125**, **127**, and **129** reported by Guo et al. have the same nomenclatures as **122**, **124**, **126**, and **128** isolated by *Niu et al. (2021a)* however, they have different structures.

From Antarctic lichen *Himantormia lugubris*, two new analogs, himantormiones A (**130**) and B (**131**) were separated and identified by *Koo et al. (2022)* Compound **130** featured propyl and pentyl units at C-1 and C-8, respectively, while **131** has two pentyl moieties. These compounds exhibited inhibitory capacity on *S. aureus* (IC$_{50}$s 35.09 and 7.01 µM) in the broth microdilution assay. *Nugraha et al. (2022)* stated that **136** reported from Indonesian lichen *Candelaria fibrosa*, had antibacterial efficacy against *B. cereus* and *S. aureus* (MICs 88.0 and 39.6 µM, respectively) in the microdilution method.

Furthermore, **139**, **142**, **144**, **145**, **150–153**, and **160** reported from *Aspergillus unguis* demonstrated potent antifungal potential against *S. cerevisiae* (ATCC 9763) (MICs 2.3–25.0 µg/mL), compared to clotrimazole (MIC 0.4 µg/mL). Besides, **142**, **144**, **145**, **158**, and **159**, along with earlier reported **138**, **139**, **146**, **147**, **150–153**, **157**, and **160** were found to have antibacterial effectiveness against *B. subtilis* and *S. aureus* (MICs 0.8–41.1 µg/mL) in comparison with ampicillin (MIC 0.2 and 3.1 µg/mL, respectively). Whilst **146**, **147**, **157**, **159**, and **160** (MICs 0.8, 1.6, 0.8, 1.6, and 0.8 µg/mL, respectively) revealed the powerful efficacy against *B. subtilis*, also **144**, **151**, **157**, **159**, and **160** with MICs 2.6, 1.6, 1.6, 3.1, and 2.9 µg/mL, respectively were the most active against *S. aureus*. Structure-activity relationship revealed the role of bromo- and/or chloro-substitution in enhancing the potency and maintaining selectivity against bacteria and yeast (*Morshed et al., 2018*).

Aspergisidone (**164**), a new metabolite, along with **138–140, 146–150, 155, 157**, and **160** were obtained from soil-associated *A. unguis* PSU-RSPG204 mycelia and broth EtOAc extract using Sephadex LH-20/SiO$_2$ CC/preparative TLC and assigned by spectral analyses (*Phainuphong et al., 2018*). Compounds **155** and **160** had powerful antibacterial influence
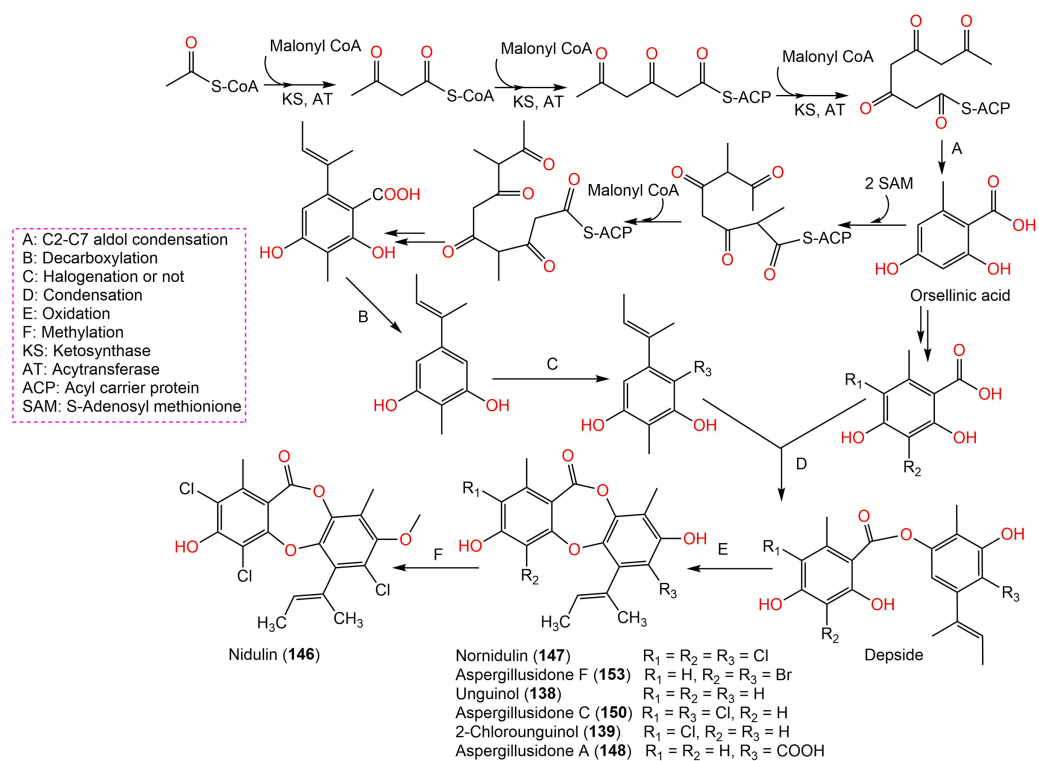
Scheme 2 Biosynthetic pathway of 138, 139, 146–148, 150, and 153 (*Yang et al., 2018*; *Sureram et al., 2013*).

against MRSA and *S. aureus* (MICs 0.5 µg/mL) as vancomycin (MICs 0.5 and 0.25 µg/mL, respectively), whereas **139**, **146, 150**, and **157** were weakly active (MIC ranged from 1–8 µg/mL). In the antifungal assay, **139** exhibited potent effectiveness on *C. albicans* (MIC 8 µg/mL), whereas **160** (MICs 0.5 µg/mL) was two-fold more effective than **157** (MIC 1 µg/mL) on flucytosine-resistant *C. neoformans* and **150** had the strongest effect on *Microsporum gypseum* (MIC 2 µg/mL) in the broth dilution method (*Phainuphong et al., 2018*). Norcolensoic acid (**132**) was purified for the first time from *Lachnum virgineum* using SiO$_2$ CC that showed intense blue color with 10% vanillin/H$_2$SO$_4$ on TLC plates. This compound displayed antimicrobial effectiveness against *Aspergillus clavatus* F318a, *S. aureus* NBRC13276, and *P. aeruginosa* ATCC-15442 (MICs 50, 25, and 25 µg/mL, respectively), however, it was inactive against *C. albicans* (*Shiono, Koseki & Koyama, 2018*). In *Yang et al. (2019)* purified depsidone analogs: **138, 139 146–148**, **150**, and **153** from plasma-mutant *Aspergillus unguis* or by *A. unguis* in a medium supplemented with epigenetic modifiers (procaine, NaBr, or procaine/NaBr) that were characterized by optical rotation, spectral, and CD analyses. These metabolites had antimicrobial efficacy against *P. aeruginosa*, MRSA, *Vibrio parahemolyticus*, and *C. albicans* (IZDs ranged 6.0 to 17.7 mm, Conc. 10 µg/disc) compared to ampicillin (IZDs 9–14 mm) and ketoconazole (IZD 22 mm for *C. albicans*), whereas **148** demonstrated potent influence on *P. aeruginosa*, MRSA, and *C. albicans*. Structure-activity relationship revealed that the ring C carboxyl group was crucial for antifungal potential (*Yang et al., 2018*). Also, **138, 139**, **146–148, 150**,

and **153** were assumed to be generated through depside production from orcinol derivatives and orsellinic acid that were derived from the PKS pathway and post-PKS modification (Scheme 2) (*Yang et al., 2018*). In previous work by *Sureram et al. (2013)*, unguinol (**138**) and aspergillusidones D–F (**151–153**) were proposed to be biosynthesized through an oxidative coupling of depsides that are produced from the condensation of orcinol derivatives (aspergillusphenols A and B) and orsellinic acid. It is noteworthy these biosynthetic intermediates were co-isolated along with these depsidones (*Sureram et al., 2013*).

Saetang et al. (2021) purified the new derivatives; asperunguissidones A (**41**) and B (**42**) in addition to **138, 139, 146–148, 150, 157, 160, 161,** and **164** from *A. unguis* PSUMF16 utilizing SiO_2/RP-10 CC/preparative TLC. All the 1-methyl-6-(2-methylbut-2-enyl) depsidone derivatives (**41, 138, 139, 146–148,** and **150**) possessed remarkable antibacterial effectiveness against *S. aureus* ATCC25923 and MRSA (MICs 1.0–8.0 μg/mL) except for non-chlorinated derivatives; **41, 138,** and **148** (*Phainuphong et al., 2018*). Structure-activity relationship revealed that C-4, C-2, and C-7 chlorination dramatically boosted antibacterial capacity. It is noteworthy that the C-4 chlorine atom remarkably elevated antifungal efficacy against *C. neoformans* (*e.g.*, **147** and **146** *vs* **150**). Moreover, **41** with 3-substituted-2-hydroxy-3-butenyl unit instead of the 2-methylbut-2-enyl unit in **138** was 2-fold more active against MRSA than **138**, however substituting H-7 (*e.g.*, **138**) with C=O group (*e.g.*, **148**) led to the loss of antibacterial potential. In the 4-methyl-1,6-di(2-methylbut-2-enyl)depsidone derivatives (**157, 160, 161,** and **164**), the non-chlorinated **157** was more potent than **138** against *S. aureus*, MRSA, and *C. neoformans* (MICs 2.0, 1.0, and 1.0 μg/mL, respectively) (*Phainuphong et al., 2018*), while **164**, the carboxyl derivative of **157** was 16-, 64-, and 64-fold less active against *S. aureus*, MRSA, and *C. neoformans* than **157**. Also, **160** (7-chloro derivative of **157**) demonstrated better potential against *S. aureus*, MRSA, and *C. neoformans* than **157** (MICs 0.5 μg/mL). Besides, lacking **161** (3-methoxy derivative of **160**) antimicrobial potential, indicating 3-OH`s importance for activity (*Saetang et al., 2021*).

A chemical investigation of marine-derived *A. unguis* EtOAc extracts using RP-18 CC and HPLC resulted in new depsidone, **156** with the known analogs, **138, 139, 143, 146, 147, 149, 155, 157,** and **160** (*Anh et al., 2022*). Compounds **156** revealed antimicrobial effectiveness against *B. subtilis*, *Micrococcus luteus*, and *S. aureus* (MICs 10.7, 10.7, and 5.3 μM, respectively), compared to kanamycin (MICs 1.0, 0.5, and 1.0 μM, respectively) in the broth dilution assay (*Anh et al., 2022*).

From coral-derived *A. unguis* GXIMD-02505, new metabolite; aspergillusidone H (**154**), along with **147, 149,** and **150** were purified by *Zhang et al. (2022)* using SiO_2/RP-18/HPLC and determined by spectral and physicochemical data. These compounds had inhibitory potential against marine biofilm-producing bacteria; MRSA, *Marinobacterium jannaschii*, *Microbulbifer variabilis*, and *Vibrio Pelagius* in the broth microdilution method. It is noteworthy that **147** possessed significant effectiveness against MRSA (MIC 2.0 μg/mL) compared to ampicillin (MIC 1.0 μg/mL). Besides, **147** and **150** exhibited moderate efficacies against *M. variabilis* and *M. jannaschii* (MICs ranged from 8.0–32.0 μg/mL) (*Zhang et al., 2022*).

Sadorn et al. (2022) reported a new metabolite; **163**, in addition to **8, 138, 139, 141, 142, 146–150, 157,** and **160–164** from *Coriandrum sativum*-associated *A. unguis* BCC-54176 using Sephadex LH-20 CC/HPLC that were assigned by spectral analyses and chemical transformation, as well as X-ray data for **163**. Compounds **8, 139**, **141**, **146**, **147**, **149**, **150**, and **160–164** displayed broad antibacterial effectiveness against *B. cereus* (MICs 1.56–25.00 µg/mL), while **163** had the potent efficacy (MIC 1.56 µg/mL) compared to rifampicin and vancomycin (MICs 0.31 and 0.08 µg/mL, respectively) (*Sadorn et al., 2022*). Assessing the anti-phytopathogens activity of these metabolites revealed that **139, 147, 150**, and **164** were active (MICs 6.25–50 µg/mL) on *Alternaria brassicicola* and **139, 141, 146–148, 150, 160**, and **164** demonstrated anti—*Colletotrichum acutatum* (MICs 3.13–50.00 µg/mL) using CFDA (5(6)-carboxyfluorescein diacetate) fluorometric assay compared to amphotericin B (MIC 1.56 µg/mL). Whilst all of them did not possess any effect on *A. baumannii* (Conc. 50 µg/mL) (*Sadorn et al., 2022*). Structure-activity relation showed that metabolites with two (E)-1-methylprop-1—enyl units at C-6 and C-1 (*e.g.*, **157** and **160–164**) and the ones with C-7 Cl-atom (*e.g.*, **160**) had more potential against *B. cereus* than the non-chlorinated analog (*e.g.*, **157**). On the other hand, compounds with C-2 and C-7 two Cl-atoms had better activity (**163** and **162**) than the compound with one Cl-atom (as in **160**). In addition, the C-3 methoxy group led to the loss of activity (**160** *vs* **161**), while the C-7 carboxy boosted the efficacy (**157** *vs* **164**). Further, more (E)-1-methylprop-1—enyl moiety and Cl-atoms in the compounds led to more activity (*Sadorn et al., 2022*).

Antimalarial and antimycobacterial activities

Compound **44** purified from *Cladonia pyxidata* was found to have marked growth inhibitory potential against *Mycobacterium tuberculosis* H37Ra and six MDR (multidrug-resistant) *M. tuberculosis* clinical isolates with MICs 7.81–31.25 µg/mL, compared to rifampicin (MICs 0.2–100 µg/mL) using the XRMA method (*Thuan et al., 2022*). Further, **65** and **136** reported from *Usnea laevis* possessed potent antimycobacterial capacity against MDR strains of *Mycobacterium smegmatis* (MDR-40 and MDR-R) (MICs 50 µg/mL) than rifampicin (MICs 100 and >200 µg/mL, respectively), also **136** had potent (MICs 50 µg/mL) efficacy towards *M. tuberculosis* (MDR-A8 and MDR-V791) compared to rifampicin (MICs 100 and >200 µg/mL, respectively) (*Tatipamula & Annam, 2022*).

Among the reported derivatives; **8, 138, 139, 141, 142, 146–150, 157**, and **160–164** from *C. sativum*-associated *A. unguis* BCC-54176, **149, 157**, and **160–163** revealed anti-*Plasmodium falciparum* (K1, MDR-strain, IC$_{50}$s 7.69–9.02 µM) in the micro-culture radio-isotope assay compared todihydroartemisinin (IC$_{50}$ 2.60 nM) and chloroquine (IC$_{50}$ 0.51 µM) (*Sadorn et al., 2022*) (Table S3), whilst **138, 139, 150, 160, 162,** and **163** exhibited anti-*Mycobacterium tuberculosis* (MICs 15.0–50 µg/mL) relative to ofloxacin, rifampicin, streptomycin, ethambutol, and isoniazid (MICs 0.39, 0.01, 0.31, 0.94, and 0.05 µg/mL, respectively) in the GFPMA (green fluorescent protein microplate assay) (*Sadorn et al., 2022*).

Cytotoxic activity

Some of the reported depsidones were assessed for their cytotoxic capacities against different cancer cell lines that were highlighted below, and the results of the potential metabolites were listed in Table S4.

Flavicansone (**19**) a 2,7-dichloro-3,8-dimethoxy-1,6,9-trimethyl-11H-dibenzo[b,e][1,4] dioxepin-11-one was separated as a new metabolite, along with **16** from *Teloschistes flavicans* lichen utilizing SiO_2 CC and Sephadex LH-20 that were specified by different spectral tools. Compound **19** is structural like **16** with differences in substitution at C-3 and C-4, having 3-OCH_3 instead of 3-OH in **16** and lacking 4-CH_3 in **16**. Compound **19** possessed moderate cytotoxic effectiveness against HL-60 cells in the CCK-8 assay (IC_{50} 58.18 μM) compared to quercetin (IC_{50} 61.1 μM) and 5-fluorouracil (IC_{50} 9.5 μM) (*Sanjaya et al., 2020*). Botryorhodine I (**26**) was reported as a new derivative, along with **18**, **21**, **22**, **24**, and **27** from sediment-obtained *Lasiodiplodia theobromae* M4.2-2 rice cultures using Sephadex LH-20 CC and HPLC. Only **18** possessed noticeable cytotoxic potential (IC_{50} 7.3 μM) on L5178Y compared to kahalalide F (IC_{50} 4.30 μM) in the MTT assay, while other metabolites were inactive (*Umeokoli et al., 2019*). The cytotoxic effectiveness of **23–25** and **88** against MMQ and GH3 cells showed that **88** had potent cytotoxic potential against GH3 and MMQ cell lines (IC_{50} 3.64 and 3.09 μM, respectively), while **23** (IC_{50}s 31.62 and 19.72 μM, respectively) displayed moderate effectiveness and **24** and **25** were inactive in the MTT assay (*Zhang et al., 2018*).

A new depsidone, curdepsidone A (**29**) purified from white croaker-associated curvularia sp. IFB-Z10 EtOAc extract by macro-porous resin CC and HPLC and assigned by spectral analyses. It displayed marked cytotoxic efficacy against BEL7402 and BEL7402/ 5-Fu (IC_{50}s 9.85 and 2.46 μM, respectively), compared to 5-fluorouracil (IC_{50}s 14.0 and 1,630.0 μM, respectively) in the MTT assay (*An et al., 2018*). A novel depsidone, bailesidone (**47**), which is an 8`S-configured analog of **69** with unparalleled B-ring substituents was biosynthesized by *Usnea baileyi*. This metabolite had moderate potential against the A549 cell line (IC_{50} 92.94 μM) and no influence against the HT-29 cell line (*Van Nguyen et al., 2018*). *Bui et al. (2022)* purified and characterized a new derivative; ceratinalone (**58**) along with **47**, **59**, **61**, and **62** using SiO_2 CC and spectral data. Compounds **58** and **61** were moderately cytotoxic against MCF-7, HeLa, HepG2, and NCI-H460 in the SRB assay. Besides, **61** revealed a notable influence against HeLa cells (IC_{50} 15.61 μg/mL) (*Ouyang et al., 2018*). Compounds **65** and **134** demonstrated high cytotoxic efficacy against DLD-1 and HCT116 cells through modulation of NF-κB, Nrf2, and STAT3 pathways. It was found that **65** was the most potent modulator of these pathways (*Papierska et al., 2021*).

The new depsidones: boremexins A–C (**82–84**), in addition to **7**, **30**, **31**, and **34** were biosynthesized by *Boeremia exigua* harboring potato that were separated and specified utilizing SiO_2/RP-18 CC/HPLC and spectral/ECD analyses, respectively. Compounds **82** and **83** were obtained as a racemic mixture having 10*R* ([α]$_D$ + 199.2) and 10*S* ([α]$_D$ − 206.5) configurations, respectively that were further separated into enantiomers on chiral
HPLC column. In the MTT assay, **83** (IC$_{50}$ 33.1 μM) possessed cytotoxic capacity against MCF–7 compared to taxol (IC$_{50}$ 0.008 μM) (*Chen et al., 2020*).

Nakashima et al. (2018) purified **86** from *Phellodendron amurense*-associated *Diaporthe* sp. ECN.137 culture by SiO$_2$ CC, which was assigned by spectral and X-ray analyses. Its effect against TGFβ1, which boosts the tumor cell invasion was examined. It was found (Conc. 20 μM) to repress TGFβ1-caused wound closing of MDA-MB-231 cells, indicating its possible potential as a tumor metastasis inhibitor (Fig. 9). On the other hand, **96** revealed prominent cytotoxic efficacy against HepG2 and HeLa cells (IC$_{50}$s 19.64 and 13.97 μg/mL, respectively), whereas **97** had better cytotoxic potential on HepG2 (IC$_{50}$ 6.83 μg/mL) in comparison to camptothecin (IC$_{50}$s 3.6 and 6.3 μg/mL, respectively) in the MTT assay (*Ouyang et al., 2018*).

A study by *Promgool et al. (2022)* showed that mollicellins **91**, **92**, **94**, **95**, **97**, **99**, **100**, **104**, and **108-110** exhibited cytotoxic efficacy against Hela, KB, HepG2, MCF-7, and HT-29 cell lines (IC$_{50}$s 4.79–92.11 μM), where **95**, **97**, and **110** (IC$_{50}$s 4.79, 10.64, and 9.83 μM, respectively) and **91**, **95**, and **110** (IC$_{50}$s 10.66, 7.10, and 11.69 μM, respectively) were potent against KB and HepG2 cell lines, respectively. These metabolites were cytotoxic on Vero cells (IC$_{50}$s 5.65–54.06 μM) except **111**. The findings indicated that the complete lactone ring and C-4-CHO group were substantial for activity, whereas the replacement of C-4-CHO with CH$_2$OH resulted in the loss of activity (*e.g.*, **111**) (*Promgool et al., 2022*).

Also, *Koo et al. (2022)* reported that in the MTS assay of **130** and **131** against HCT-116 cells, **131** showed potent cytotoxic potential (EC$_{50}$ 1.11 μM) than 5—fluorouracil (EC$_{50}$ 9.4 μM), suggesting its potential as an anticancer lead against colon cancer. Additionally, physodic acid (**134**) identified from *Hypogymnia physodes* European lichen (Fig. 11) was found to exhibit cytotoxic potential against A-172, T98G, and U-138 MG cell lines (IC$_{50}$s 42.41, 50.57, and 45.72 μM, respectively) in the MTT assay (*Studzińska-Sroka et al., 2021*). Additionally, Cardile et al. investigated **134**`s potential on DU-145 and LNCaP cell growth and its apoptotic capacity on TRAIL-resistant LNCaP cells in combination with TRAIL (tumor-necrosis factor-related apoptosis-inducing ligand) using MTT assay. Lactate dehydrogenase (LDH) release is a marker of membrane breakdown. It prohibited both cell viability (Conc. 12.5–50 μM) without affecting normal cells and no observed increase in LDH (lactate dehydrogenase) level, which is a marker for membrane integrity. In addition, it activated apoptosis and raised ROS formation. Interestingly, it sensitized LNCaP cells to TRAIL-produced apoptosis. Thus, combining **134** with other anti-prostatic cancer drugs could be a prominent treatment strategy that required further studies (*Cardile et al., 2022*).

Anh et al. (2022) stated that **138**, **139**, **143**, **146**, **147**, **155–157**, and **160** were found to have cytotoxic potential against PC-3, NCI-H23, HCT-15, NUGC-3, ACHN, and MDA-MB-231 with IC$_{50}$s ranging from 3.4 to 27.7 μM, whereas **138**, **139**, and **143** were the most potential metabolites (IC$_{50}$s 3.4–6.2 μM). It was observed that the number of chlorine and substitution had no significant effect on activity, while free C-4-OH (**157**) was substantial for activity.

Zwartsen et al. (2019) reported that **138** and **151** reduced MDA-MB-231 cell viability (Conc. M50 μM), while they did not affect cell proliferation (Fig. 12). Additionally, they caused MDA-MB-231 cell cycle arrest (Conc. 100 μM). It is noteworthy that **138** potency

was less than **151**, this variation may be due to two bromine atoms in **151** compared to **138** that enabled the halogen bonds formation (Fig. 12).

New depsidones: **142**, **144**, **145**, **158**, and **159**, along with earlier reported **138**, **139**, **146**, **147**, **150**-**153**, **157**, and **160** were biosynthesized by *A. unguis* using yeast extract sucrose culture media supplemented with KBr or NaCl (*Morshed et al., 2018*). In the MTT assay, they demonstrated cytotoxic potential against NS-1 cell line (MICs 6.3 to 50 µg/mL) compared to 5-fluorouracil (MIC 0.1 µg/mL), whereas **138**, **157**, **159**, and **160** (MICs 12.5, 6.3, 12.5, and 12.5 µg/mL, respectively) were the most active (*Morshed et al., 2018*).

Phainuphong et al. (2018) reported that **160** revealed the potent inhibition activity on HCT-116 cell (IC$_{50}$ 23.5 µM, inhibition 87.06%), while **138**–**140**, **146**–**150**, **155**, **157**, and **164** had weak to moderate efficacy (3.98–59.63%). Compound **160** also dose-dependently decreased (IC$_{50}$s 34.8–84.7 µM) live cells/dead cells numbers in a 3D-culture model relying on the incubation durations, indicating its potential in spheroidal cancer model (*Phainuphong et al., 2018*). Further, compounds **146**, **147**, and **153** demonstrated notable larvicidal potential on *Artemia salina* (LC$_{50}$s 4.5–12.8µM) compared to Hg(NO3)$_2$ (LC$_{50}$ 77.0 µM) (*Yang et al., 2018*).

Compounds **112**–**114** and **165**–**167** separated from the culture of wetland-soil-associated *Pycnidiophora dispersa*, utilizing SiO$_2$/RP-18 CC/HPLC had cytotoxic capacity against HeLa, PC-3, A549, HepG-2, and HL-60 (IC$_{50}$s ranged from 11.4 to 86.8 µM) compared to cisplatin (IC$_{50}$s ranging from 5.6 to 15.7 µM) in the CCK-8 assay. Compounds **112** and **165** had marked efficacy on A549 cells (IC$_{50}$s 13.0 and 11.4 µM, respectively) compared to cisplatin (IC$_{50}$ 11.8 µM) (*Zhao et al., 2020*).

From *Garcinia paucinervis* stems, a new depsidone, paucinervin Q (**169**) was separated by SiO$_2$ and RP-18 CC and assigned by spectral analyses. This compound revealed marked inhibition capacity against PC-3, HL-60, and CaCo-2 (IC$_{50}$s 18.57, 3.11, and 6.78 µM, respectively) in the MTT assay compared to 5-fluorouracil (IC$_{50}$s 30.59, 2.39, and 38.77 µM, respectively) (*Jia et al., 2019*) (Fig. 13).

Anti-inflammatory activity

Inflammation is a complicated defense process, which is induced by pro-inflammatory cytokines secretion by macrophages as a result of stimuli (*e.g.*, infectious agent, tissue ischemia, injury, *etc.*) (*Zhao et al., 2021a*; *Liang et al., 2022*). Impairment of the pro-inflammation mediator secretion can lead to diverse disorders such as asthma, atherosclerosis, psoriasis, periodontal diseases, carcinogenesis, and rheumatoid arthritis (*Chen et al., 2018a*; *Niu et al., 2021b*).

Also, polyanthadepsidone A (**1**), a new highly methylated depsidone from the *Garcinia polyantha* leaves dichloromethane extract exhibited *in vitro* suppressive influence on the oxidative burst by serum opsonized zymosan in the whole blood (*Lannang et al., 2018*).

Chemical investigation guided by HPLC/DAD of the EtOAc extract of the marine-derived *Curvularia* sp. IFBZ10 resulted in new depsidones; **30**–**35** that were separated by SiO$_2$ CC/HPLC and their structures and absolute configuration were determined by spectral analyses as well as TDDFT/ECD (time-dependent density functional theory/electronic circular dichroism) and DFT/NMR (density functional

theory/nuclear magnetic resonance) calculations (*Duong, 2019*). The anti-inflammation potential of **30**, **31**, **34**, and **35** was assessed by measuring IL-1β production inhibition in *Propionibacterium acnes*-induced THP-1 cells. Compound **31** exhibited noticeable IL-1β production inhibition (IC_{50} 7.47 μM) compared to retinoic acid (IC_{50} 3.38 μM), while **30** and **35** (IC_{50} 18.83 μM) had no and moderate efficacy, respectively revealing that stereo-configuration had a substantial role in the activity. Further, **31** prohibited the IL-1β production by selectively minimizing the JNK and ERK phosphorylation. The molecular docking implied that **31** suppressed IL-1β production *via* binding to the TLR2/1 protein active site (*Ding et al., 2019*). Compounds **7**, **34**, and **82–84** revealed anti-inflammation potential (IC_{50}s 19.4–34.4 μM) on NO formation induced by LPS in RAW264.7 macrophages, where **7** and **83** had potent potential (IC_{50}s 22.6 and 19.9 μM, respectively) relative to PDTC (IC_{50} 23.1 μM, ammonium pyrrolidine dithiocarbamate) (*Chen et al., 2020*) (Table S5).

Hao et al. (2022) purified compound **55**, a new tetracyclic derivative from mangrove-associated *Aspergillus* sp. GXNU-A9 EtOAc extract utilizing SiO_2 CC and HPLC. This metabolite (IC_{50} 8.22 μM) displayed a noticeable NO production inhibition capacity in RAW 264.7 cells boosted by LPS compared to dexamethasone (IC_{50} 5.62 μM). In another study, *He et al. (2022)* investigated *Melastoma malabathricum subsp. normale* roots utilizing SiO_2/RP-18/Sephadex LH-20 CC/HPLC, resulting in a new derivative, guanxidone B (**56**) together with **12**, **51**, and **55**. Their structures were elucidated by spectral and CD analyses. Compounds **55** and **56** possessed marked anti-inflammation efficacy (IC_{50}s 6.46 to 9.82 μM, respectively) *via* suppressing NO production utilizing Griess Reagent System compared to dexamethasone (IC_{50} 2.52 μM). Compound **56** was structurally similar to **51** having C-4 CH_2OH instead of C-4 CH_3 in **51**. It is noteworthy that **56** had better activity than **55**, indicating that CH_3O at C-4 affected the activity (*He et al., 2022*).

Lobaric acid (**136**) separated from *Stereocaulon paschale* nordic lichen was found to prohibit TNF-α and IL-1β secretion and NF-κB activation boosted by LPS in macrophages. Docking results revealed its binding to PPAR-γ between beta-sheet and helix H3 as a partial PPAR-γ agonist, suggesting its efficacy because of NF-κB pathway blockage *via* PPAR-γ activation (*Carpentier et al., 2018*). These findings supported the development of **136** as PPAR-γ agonists for chronic inflammation disorders. From *Usnea subfloridana*, salazinic acid (**65**), galbinic acid (**49**), lobaric acid (**136**), conprotocetraric acid (**173**), and constictic acid (**174**) exerted antigout and antiinflammation capacities through inhibition of 5-LOX, COX1, XO, and COX2 in enzyme inhibition assays. It is noteworthy that **136** and **173** had effective COX2 inhibition capacity (IC_{50}s 7.01 and 7.17 μM, respectively), compared to indomethacin (7.3 μM), whereas all of them exhibited potent XO inhibition activity (*Nguyen et al., 2021*).

Anti-*Helicobacter pylori* activity

The inhibition of *Helicobacter pylori* urease activity is an effective strategy for treating this infectious disease. From *Cladonia rappii* acetone extract, **44** was separated by crystallization (($CH_3)_2$CO:$CHCl_3$ 20:1) and identified by spectral data. This compound
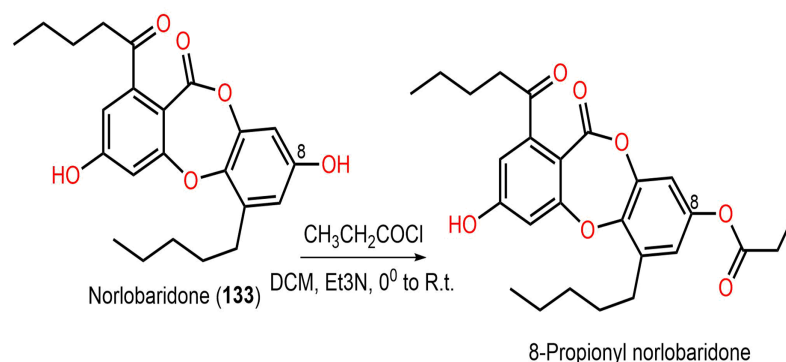
Scheme 3 Semi-synthesis of norlobaridone (**133**) derivative (*Pavan Kumar et al., 2020*).

was a marked competitive inhibitor of jack bean urease uricolytic activity. Also, it had a potent (MICs 0.034 to 0.068 µM) growth inhibition effectiveness against six clinical isolates of *H. pylori* than omeprazole (MICs 0.046–0.093 µM) in the broth microdilution assay. Therefore, **44** could be further developed for treating *H. pylori*-linked infections (*Lage et al., 2018*).

Antioxidant activity

Methylstictic acid (**61**) having β-orcinol core with γ-lactone connected to B ring and aldehyde group at C-3 was separated using SiO_2 CC and HPLC for the first time from *Hypotrachyna caraccensis*. It had reactivity and potency as DPPH• scavenger as indicated by a kinetic study (EC_{50} 2.66 µM) compared to BHT (EC_{50} 0.11 µM) and ascorbic acid (EC_{50} 0.24 µM). It had optimal lipophilicity and permeability for penetrating the skin that could be utilized as a topical component for preventing oxidative injuries (*Leal et al., 2018*). The finding of antioxidant testing in the DPPH assay of mollicellins **96–98** and **101–104** showed that only **101** exhibited weak activity (IC_{50} 71.92 µg/mL) compared to BHT (IC_{50} 0.15 µg/mL) (*Ouyang et al., 2018*). Also, **134** possessed (IC_{50} 160 µg/mL) 5-times less antioxidant potential than resveratrol (IC_{50} 31.0 µg/mL) in the CUPRAC (CUPric-reducing-antioxidant capacity) assay (*Studzińska-Sroka et al., 2021*).

Ramalina lichenized fungi depsidones; **9–11, 17, 50, 57, 59, 60, 65, 72, 73**, and **134** were examined for antioxidant properties utilizing kinetic and thermodynamic calculations in the gaseous phase and aqueous solution. It was found that their BDE (bond-dissociation-energy) values were 74.4–87.7 kcal/mol, whereas **65, 72**, and **73** had the lowest BDE(C-H)s (76.9, 74.4, and 75.2 kcal/mol^{-1}, respectively). These metabolites were significant O_2•− and HO• radical scavengers in aqueous media. Thus, depsidones exhibited potential O_2•− and HO• radical scavenging capacity (*Bay et al., 2020*). In a study by *Pavan Kumar et al. (2020)*, **133** isolated from *Parmotrema tinctorum* by SiO_2 CC, along with its semi-synthesized derivative that was prepared using propionyl chloride were assessed for antioxidant potential in ABTS assay (Scheme 3). It was observed that **133** demonstrated potent effectiveness (%ABTS inhibition 98.90%, SC_{50} 20 µg/mL) compared to trolox (%ABTS inhibition 99.78%), while its derivative was inactive (%ABTS inhibition 4.7%, SC_{50} 20 µg/

mL), revealing the importance of the free 8-OH group for the activity (*Pavan Kumar et al., 2020*).

Antidiabetic activity

Diabetes mellitus is a worldwide rapidly disseminated metabolic disorder that is distinguished by persistent hyperglycemia because of the flaw in insulin action, insulin secretion, or both (*Devi et al., 2020*). Unrestrained hyperglycemia promotes protein glycation product formation (advanced-glycation-end products, AGEs). AGEs immoderate accumulation in diabetics enhances diabetic complication pathogenesis, including nephropathy, retinopathy, cardiomyopathy, and neuropathy. It was estimated that the number of diabetic patients has been rose from 108 million in 1980 to 422 million in 2014 (*Zheng, Ley & Hu, 2018*). In 2015, five million deaths were reported due to diabetes and its related complications, making it 9th causal factor of diminished life expectancy (*Abubakar, Tillmann & Banerjee, 2015*). In 2019, two million deaths were recorded caused by diabetes, and kidney diseases resulted from diabetes (*World Health Organization, 2021*). The available oral synthetic antidiabetics *e.g.*, thiazolidinediones, biguanides, meglitinides, and sulfonylureas were reported to produce unwanted effects (*Lorenzati et al., 2010*). Thus, searching for new targets and approaches for treating diabetes is extremely recommended. α-Glucosidase (AG) is one of the fundamental enzymes implicated in carbohydrate digestion. It has been proven as an efficient target for diabetes management. However, the usage of the available alpha-glucosidase inhibitors (AGIs) such as miglitol, voglibose, 1-deoxynojirimycin, and acarbose has frequently been accompanied by side effects, in addition to the high costs. Many studies were carried out for identifying and validating the potential of natural products as AGIs for the prevention or curing of diabetes (*Assefa et al., 2019*).

The new derivatives, **54**, **67**, and **78**, along with **49** and **65** purified from *Parmotrema dilatatum* whole thalli acetone extract using SiO_2 CC were assayed for their AG inhibition activities. Compounds **54**, **65**, and **78** revealed a notable AG inhibition (IC_{50}s 2.2, 34.8, and 4.3 μM, respectively) while **49** and **67** were inactive compared with acarbose (IC_{50} 449 μM) (*Devi et al., 2020*). Structure-activity relation demonstrated the 3`-benzyl and C-3 aldehyde moieties enhanced the activity, while methylation of 8′-OH resulted in losing activity and γ-butyrolactone moiety did not influence the efficacy (*Devi et al., 2020*). Additionally, **53, 76, 77, 79**, and **80** new members of the depsidone family were separated from *Parmotrema tsavoense* utilizing SiO_2 CC/TLC and assigned by spectral methods. Compound **80** is a 2*H*-chromene containing depsidone. Investigating AGI potential of **53**, **76**, and **77** revealed their marked inhibitory effectiveness (IC_{50}s 11.4, 17.6, and 10.7 μM, respectively) than acarbose (IC_{50} 449 μM) in the colorimetric assay (*Duong et al., 2020*). Further investigation of *P. tsavoense* by *Nguyen et al. (2022a)* led to the separation of a new metabolite, **81** that demonstrated a powerful (IC_{50} 3.12 μM) AGI capacity than acarbose (IC_{50} 162.54 μM). Co-culturing of *Trichoderma* sp. 307 derived from *Clerodendrum inerme* with *Acinetobacter johnsonii* B2A (pathogenic aquatic bacteria) produced a new depsidone, botryorhodine H (**88**) and known analogs, **23–25** that were separated and characterized using Sephadex LH-20 and SiO_2 CC and spectral analyses, respectively.
These metabolites possessed powerful AG inhibition capacity (IC_{50}s 8.1, 11.2, and 10.3 µM, respectively) than acarbose (IC_{50} 703.8 µM), whereas **25** displayed 13-fold more inhibition capacity (IC_{50} 54.1 µM) than acarbose (Table S6). It was indicated that C-3 functional groups influenced AGI activity (**88** *vs* **24** *vs* **25**), while the C-3′ CH_3 group did not affect the activity (**23** *vs* **24**) (*Zhang et al., 2018*).

Antihypertensive activity

RhoA (Ras homolog-gene-family-member-A) is a member of the Rho—GTPase superfamily that was originally found to promote migration and cell cycle progress in cancer cells and control actin dynamics that are substantial for preserving the cell's cytoarchitecture. It had been reported to have a marked role in cardiomyopathies and cardiac remodeling (*Kilian et al., 2021*). Also, the inhibition of RhoA activation reduced the angiotensin II-dependent hypertension development (*Olivon et al., 2018*). Olivon et al. identified the new metabolite, baillonic acid (**20**) along with **59** from New Caledonian *Meiogyne baillonii* bark EtOAc extract. Only **59** exhibited a significant RhoA-p115 complex GDP/GTP exchange inhibition potential (IC_{50} 187 µM, 50.5% inhibition) in the Biacore assay, thus it could have a potential for treating high blood pressure (*Olivon et al., 2018*).

Anti-diarrheal activity

CFTR (cystic fibrosis transmembrane conductance regulator) is a cAMP-activated chloride channel that is accountable for the trans-epithelial secretion of chloride, resulting in the promoting force for intestinal fluid secretion (*Li & Naren, 2010*). The CFTR's excessive function leads to secretory diarrhea, therefore its prohibition minimized intestinal fluid secretion. The CFTR inhibitory potential of **138**, **139**, **141**, **146**, **147**, **150**, **157**, **160**, and **164** in T84 cell monolayers using short-circuit current analysis was estimated. It is noteworthy that **138**, **139**, **141**, **147**, **150**, **157**, and **160** had remarkable (concentration 10 µM, >50% inhibition) CFTR-mediated chloride secretion inhibition where **160** and **157** were the most powerful. Compounds **157** and **160** dose-dependently prohibited forskolin-boosted chloride secretion in T84 cells (IC_{50}s 0.5 and 2.0 µM, respectively) with almost complete suppression at concentrations of 20 and 10 µM, respectively, whereas **157** was more potent than **160**. Further investigation of **157** for their effect on CT (cholera toxin)-boosted chloride secretion across T84 cells. CT is an enterotoxin accountable for massive symptoms of cholera patients' diarrhea. Compound **157** was found to dose-dependently prohibit CT-induced chloride secretion (IC_{50} 5.0 µM) with complete prohibition at a concentration of 100 µM. These findings revealed an anti-secretory potential of **157** and **160** that could be beneficial for diarrhea treatment (*Phainuphong et al., 2018*).

BChE (butyrylcholinesterase) and AChE (acetylcholinesterase), and phosphodiesterase inhibition activities

Neurodegenerative illnesses, such as Alzheimer's (AD) or Parkinson's disease (PD) represent a critical global health concern. They are a series of procedures that result in the

gradual forfeiture of neuronal function and nerve cell death (*Di Paolo et al., 2019*). BChE (butyrylcholinesterase) and AChE (acetylcholinesterase) are substantial for CNS functions that hydrolyze acetylcholine (*Studzińska-Sroka et al., 2021*). Acetylcholine hydrolysis suppression is substantial in neuro-degenerative illnesses. Moreover, BChE and AChE noncholinergic actions like the impact on cellular adhesion and proliferation process regulation are also crucial in brain tumors (*Studzińska-Sroka et al., 2021*).

Rukachaisirikul et al. (2019) stated that **23** and **27** possessed PDE5 (−5) inhibition capacity (% inhibition 84% and 89% and IC_{50}s 5.69 and 9.96 µM, respectively). Studzińska-Sroka et al. investigated **134** AChE and BChE inhibition potentials using Ellman's colorimetric method. It only prohibited BChE (%inhibition 8.1%) (*Studzińska-Sroka et al., 2021*). Compound **148** reported from *A. unguis* displayed AChE inhibition potential (IC_{50} 102.4 µM), while **138**, **139**, **146**, **147**, **150,** and **153** had weak or no effectiveness (*Yang et al., 2018*).

Tyrosinase and hyaluronidase inhibitory activities

Hyaluronic acid (HA) is a brain-extracellular matrix prime component that is generated by Hyaluronan synthase (HAS) and broken down into fragments by hyaluronidase (*Misra et al., 2011*). The resulting fragments were reported to be related to enhanced cancer cell invasion capability and proliferation, as well as proangiogenic and proinflammation processes (*Chen et al., 2018b*).

Studzińska-Sroka et al. (2021) stated that **134** had a high hyaluronidase suppression potential with IC_{50} 0.053 mg/mL that was 6–10 times more powerful than tannic acid (IC_{50} 0.554 mg/mL).

Tyrosinase oxidizes surplus dopamine to form dopamine quinones, quite reactive species that promote cell death and neural damage. It is implicated in neurodegeneration-related illnesses like Parkinson's disease (*Chen et al., 2018b*). Thus, its prohibition is targeted to discover new drugs for these disorders, particularly Parkinson's disease. Compound **134** showed 25% inhibition of tyrosinase enzyme (Conc. 1.6 mg/mL), which was 3-times lower than azelaic acid using L-DOPA (substrate) (*Studzińska-Sroka et al., 2021*).

Anti-osteoclastogenic activity

Bone homeostasis is maintained and regulated by two metabolic processes, bone formation by osteoblasts and bone resorption by osteoclasts (*Jacome-Galarza et al., 2019*). Osteoclast differentiation is controlled by two factors, the M-CSF (macrophage colony stimulation factor) and RANKL (receptor activator of the nuclear factor kappa-B ligand). Signaling pathways of RANKL are considered key targets for prohibiting bone resorption and osteoclast differentiation (*Tan et al., 2020*). NF-κB has a pivotal function in RANKL-caused osteoclast differentiation (*Zhang et al., 2022*).

Zhang et al. (2022) investigated the inhibitory potential of **147**, **149**, 150, and **154** on RANKL-induced osteo-clastogenesis in RAW264.7 macrophages and BMMs (bone marrow macrophage cells) using luciferase reporter gene and TRAP (tartate-resisant acid
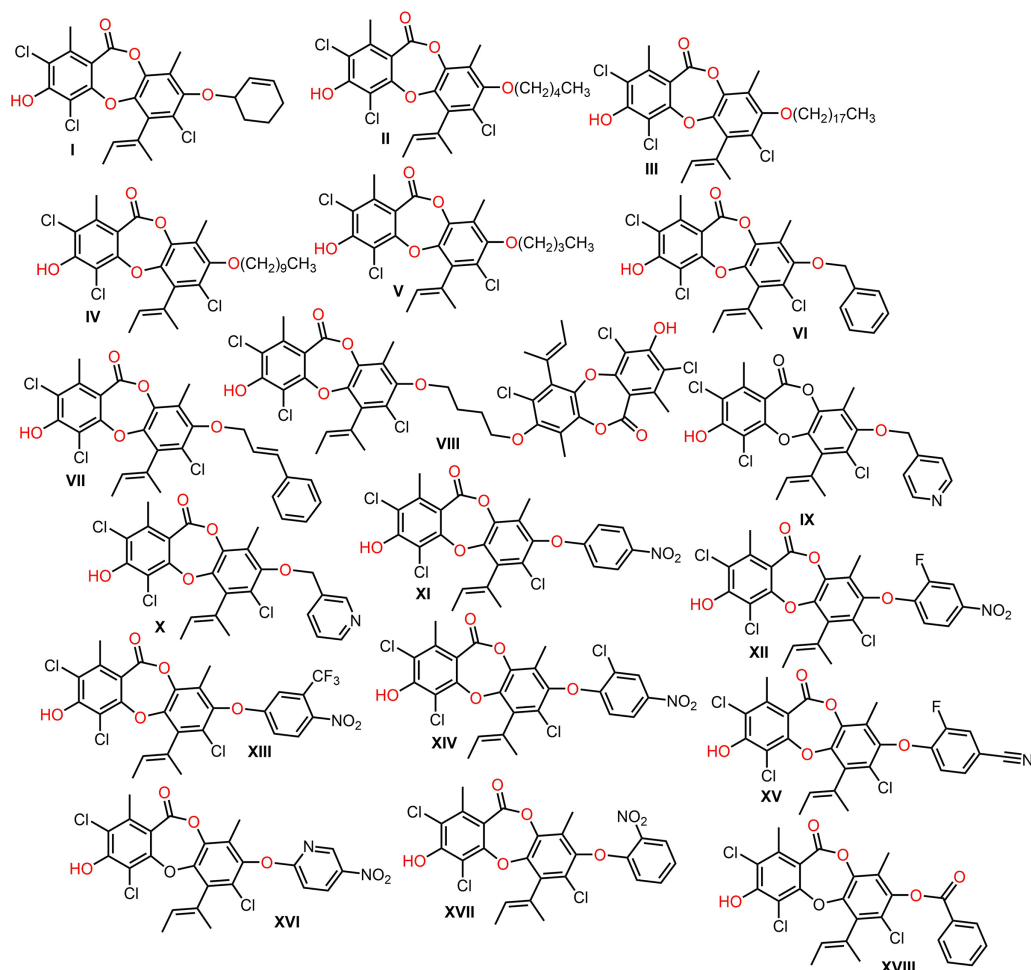
Figure 14 Semisynthetic derivatives of nornidulin (I–XVIII).

phosphatase) assays, respectively. It was found that **147**, **149**, and **154** demonstrated prohibition of LPS-caused NF-κB activation in RAW264.7 macrophages (Conc. 20 μM).

Phytotoxic activity

Norcolensoic acid (**132**) was found to prohibit lettuce seedlings' root growth (% inhibition 92 and 63%, respectively at Conc. 300 and 100 μg/mL, respectively), whereas it strongly suppressed seed germination at a concentration of 500 μg/mL (*Shiono, Koseki & Koyama, 2018*).

Antiviral activity

Cordia millenii investigation resulted in a new analog, **6** that was assigned by spectral and X-ray analyses. This compound had promising HIV-1 integrase efficacy (IC$_{50}$ 4.65 μM) in comparison to chicoric acid (IC$_{50}$ 0.33 μM) (*Dongmo Zeukang et al., 2019*).

Salazinic (**65**) and protocetraric (**17**) acids were reported as 3CLpro SARS-CoV-2 slow-binding inactivators (*Ki* of 3.77 and 3.95 μM, respectively) that could be possible
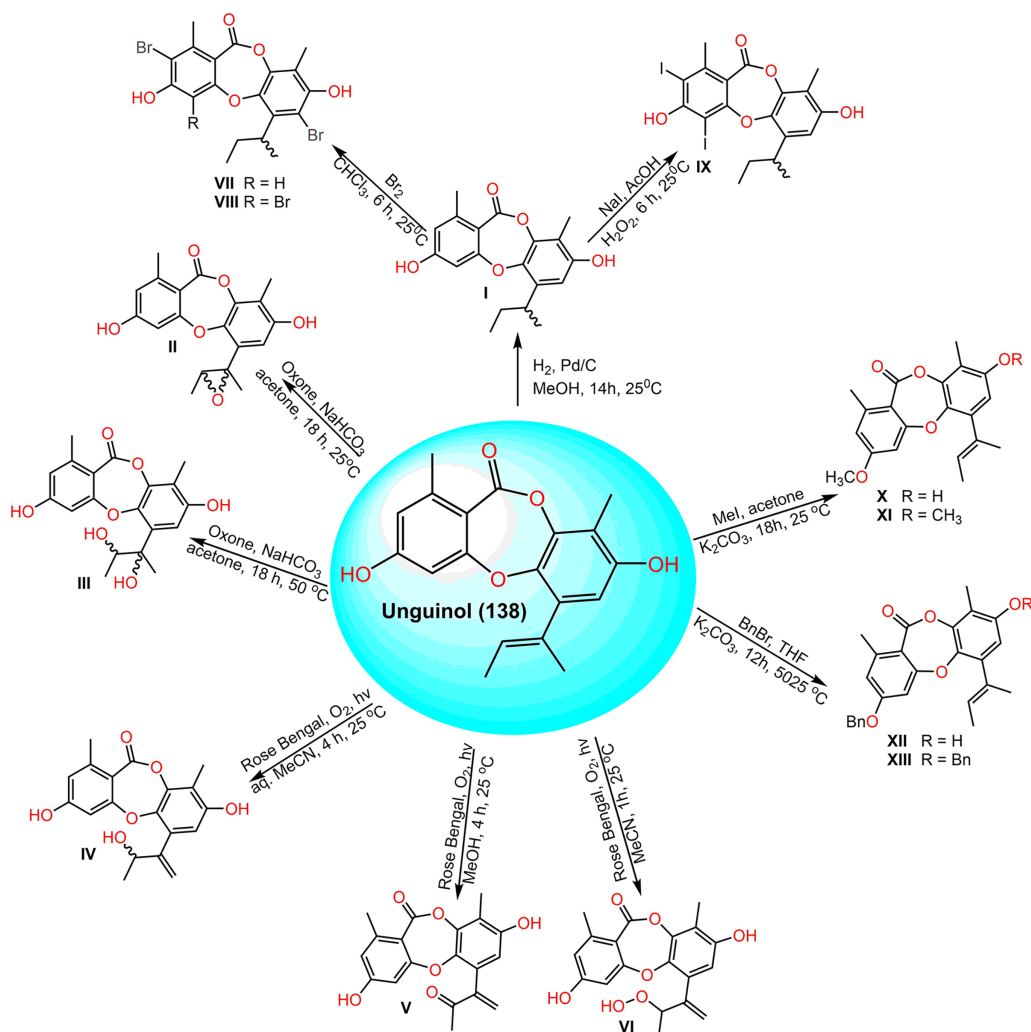
Scheme 4 Semisynthetic derivatives (I–XIII) of unguinol (138) (*Morshed et al., 2021*).

scaffolds for the development of effective SARS-CoV-2 cysteine enzyme 3CLpro inhibitors (*Fagnani et al., 2022*).

GnRH (Gonadotropin-releasing hormone) antagonistic activity

Nguyen et al. (2022b) proved that the treatment of female rats with lobaric acid (**136**) (50 and 100 mg/kg b.w./day) significantly ameliorated tetramethrin (50 mg/kg b.w/day)-induced alteration on estrous cycle. It reversed gonadotropins serum levels through influencing the pituitary/hypothalamic axis and competitively inhibited tetramethrin binding to GnRH receptor in both thermodynamic and kinetic processes.

SEMISYNTHETIC DEPSIDONE DERIVATIVES

Isaka et al. (2019) synthesized derivatives of **146** utilizing regioselective arylation, acylation, and alkylation reactions to give 8-O-substituted analogs that were assessed for their antibacterial potential. Many of the 8-O-alkyl derivatives had more powerful

antibacterial capacities than **146**, whereas 8-O-butyl exhibited the highest potential against *B. cereus* (MIC 0.391 µg/mL), however, the derivatives with long sidechains, as well as acylated derivatives displayed weaker capacity. On the other hand, O-aryl analogs demonstrated powerful antibacterial potential against MRSA (*Isaka et al., 2019*) (Fig. 14).

Morshed et al. (2021) prepared semisynthetic derivatives of **138** (Scheme 4). Among them, 3-O-(2,4-difluorobenzyl)unguinol and 3-O-(2-fluorobenzyl)unguinol possessed remarkable antibacterial effectiveness against methicillin-susceptible and -resistant *S. aureus* (MIC 0.25–1 µg/mL).

CONCLUSION

Natural metabolites biosynthesized by various living organisms are renowned for their vital contribution to drug design and discovery. In this work, a total of 172 depsidones were reported from various sources from 2018 to 2022 with a greater number separated in 2022. The major depsidone derivatives are reported from fungi (107 compounds, 62.2%), then lichens (52 compounds, 30.3%), and the least number of depsidones were reported from plant sources (13 compounds, 7.5%). These metabolites were commonly separated from the species belonging to the following genera: *Aspergillus*, *Chaetomium*, and *Spiromastix* (fungi); *Usnea*, *Parmotrema*, and *Ramalina* (lichens), and *Melastoma*, *Hypericum*, and *Garcinia* (plants).

It is noteworthy that these metabolites show various structural features according to their sources. It was noted that fungal-derived depsidones possess various substituents such as pyran (*e.g.*, **83**, **86**, **91**, **99**, **100**, and **102–104**), substituted benzyl (*e.g.*, **88–90**), isoprenyl (*e.g.*, **92–94**, **96–98**, and **105–111**), 2-methylbut-2-enyl (*e.g.*, **138–167**), three to five carbon aliphatic chain (*e.g.*, **115–129**), and halogen (bromine (*e.g.*, **121**, **123**, **125**, **127**, **129**, **144**, **145**, **151**, **152**, and **159**) and chlorine (*e.g.*, **116–120**, **139–144**, **154–156**, and **160–163**)) and lichen-derived depsidones feature furan (*e.g.*, **45–52** and **57–73**), substituted benzyl (*e.g.*, **54** and **74–79**), and five to seven aliphatic chains (*e.g.*, **130–137**), while that reported from the plant have isoprenyl substituent (*e.g.*, **168–170**).

These metabolites were evaluated for various bioactivities mainly antimicrobial, cytotoxic, and antidiabetic capacities. Depsidones could have the potential as lead metabolites for neurodegenerative illnesses and diabetes through their inhibition of butyrylcholinesterase, tyrosinase, α-glucosidase, and acetylcholinesterase enzymes. Besides, **127** could be a potential lead for bactericides to control rice bacterial-blight disease. Also, **44** demonstrated powerful anti-*H. pylori* potential that could be further developed for treating *H. pylori*-linked infections. It was found that the ring substation patterns greatly influenced the activities as highlighted in some reports on structure-activity relation (*Shukla et al., 2019*; *Niu et al., 2021b*).

Preparation of semi-synthetic derivatives from these compounds resulted in derivatives with more powerful activity than parent compounds *e.g.*, unguinol and nidulin, which could encourage medicinal chemists to carry out further modification of the structures of other reported metabolites and assess the effect of this modification on the bioactivities. Besides, altering cultural media conditions could be an efficient strategy to get novel biometabolites. Also, the co-culturing of two or more organisms from different species

produced interesting metabolites that have not been produced in the cultivation of the organism alone. Therefore, this approach could be further utilized for discovering more valuable metabolites. Collectively, depsidone derivatives feature diversified chemical entities and numerous bioactivities. These metabolites could be beneficial scaffolds and building blocks for synthesizing various drugs for multiple human health disorders. However, the *in vivo* evaluation of their potential biological properties and mechanistic investigations should indubitably be the focal point of future studies.

LIST OF ABBREVIATIONS

A-172	Glioblastoma cell line
A549	Human lung adenocarcinoma epithelial cell line
ABTS	2,2`-Azinobis-(3-ethylbenzthiazoline-6-sulphonate)
ACHN	Human renal carcinoma cell lines
AChE	Acetylcholinesterase
Bel-7402	Human hepatocellular carcinoma cell line
BHT	Butylated hydroxytoluene
CCK-8	Cell counting kit-8
CD	Circular dichroism
CFTR	Cystic fibrosis transmembrane conductance regulator
CH_2Cl_2	Dichloromethane
COX1	Cyclooxygenase-1
COX2	Cyclooxygenase-2
DPPH	1,1-Diphenyl-2-picrylhydrazyl
EC_{50}	Half maximal effective concentration
ECD	Electronic circular dichroism
EtOH	Ethanol
EtOAc	Ethyl acetate
ESI-MS	Electrospray ionization mass spectrometry
GFPMA	Green fluorescent protein microplate assay
HCT-15	Human colon cancer cell line
HCT-116	Human colon cancer cell line
HeLa	Human cervical epitheloid carcinoma cell line
HepG2	Human hepatocellular liver carcinoma cell line
HPLC	High-performance liquid chromatography
HRESIMS	High resolution electrospray ionization mass spectroscopy
HT-29	Human colon cancer cell line
IC_{50}	Half-maximal inhibitory concentration
IL-1β	Interleukin-1β
KB	Human oral epidermoid carcinoma cell line
LC_{50}	Lethal concentration that kills 50%
IR	Infrared
LPS	Lipopolysaccharide

5-LOX	5-Lipooxygenase
MCF-7	Human breast adenocarcinoma cell line
MDR	Multidrug-resistant
MDA-MB	
-231	Human breast cancer cell line
Med25	Mediator of RNA polymerase II transcription subunit 25
MeOH	Methanol
MIC	Minimum inhibitory concentration
MRSA	Methicillin-resistant *Staphylococcus aureus*
MS	Mass spectrometry
MTS	(3-(4,5-Dimethylthiazol-2-yl)-5-(3-carboxymethoxyphenyl)-2-(4-sulfophenyl)-2H-tetrazoliuminner salt)
MTT	3-(4,5-Dimethylthiazol-2-yl)-2,5-diphenyltetrazolium bromide
TM4 cells	Murine Sertoli cells
NCI-H460	Human non-small cell lung cancer cell line
NCI-H187	Human small-cell lung cancer
NCI-H23	Human lung cancer cell line
NF-κB	Nuclear factor kappa-light-chain-enhancer of activated B cells
NMR	Nuclear magnetic resonance
NUGC-3	Human stomach cancer cell line
NO	Nitric oxide
PC-3	Human prostatic-testosterone-independent cell line
PDE5	Phosphodiesterase
ROS	Reactive oxygen species
PPAR-γ	Peroxisome proliferator—activated receptor gamma
RP-18	Reversed phase-18
SC$_{50}$	Scavenging concentration 50%
SiO$_2$ CC	Silica gel column chromatography
PPIs	Protein-protein interactions
T98G	Glioblastoma cell line
TLC	Thin layer chromatography
TNF-α	Tumor necrosis factor alpha
TRAIL	Tumor necrosis factor-related apoptosis-inducing ligand
U-138MG	Glioblastoma cell line
U937	Pro-monocytic, human myeloid leukemia cell line
Vero cell	Normal African green monkey kidney fibroblasts
XO	xanthine oxidase
XRMA	2,3-bis-(2-methoxy-4-nitro-5-sulfophenyl)-2H-tetrazolium-5-carboxanilide (XTT) reduction menadione assay.

Funding
The authors received no funding for this work.

Competing Interests
The authors declare that they have no competing interests.

Author Contributions
- Maan T. Khayat performed the experiments, prepared figures and/or tables, authored or reviewed drafts of the article, and approved the final draft.
- Kholoud F. Ghazawi performed the experiments, prepared figures and/or tables, authored or reviewed drafts of the article, and approved the final draft.
- Waad A. Samman performed the experiments, prepared figures and/or tables, authored or reviewed drafts of the article, and approved the final draft.
- Aisha A. Alhaddad performed the experiments, prepared figures and/or tables, authored or reviewed drafts of the article, and approved the final draft.
- Gamal A. Mohamed conceived and designed the experiments, performed the experiments, analyzed the data, prepared figures and/or tables, authored or reviewed drafts of the article, and approved the final draft.
- Sabrin R. M. Ibrahim conceived and designed the experiments, performed the experiments, analyzed the data, prepared figures and/or tables, authored or reviewed drafts of the article, and approved the final draft.

Data Availability
This is a literature review.

Supplemental Information
Supplemental information for this article can be found online at http://dx.doi.org/10.7717/peerj.15394#supplemental-information.

REFERENCES

Abdel-Razek AS, El-Naggar ME, Allam A, Morsy OM, Othman SI. 2020. Microbial natural products in drug discovery. *Processes* **8(4)**:470 DOI 10.3390/pr8040470.

Abubakar II, Tillmann T, Banerjee A. 2015. Global, regional, and national age-sex specific all-cause and cause-specific mortality for 240 causes of death, 1990–2013: a systematic analysis for the global burden of disease study 2013. *Lancet* **385(9963)**:117–171 DOI 10.1016/S0140-6736(14)61682-2.

Addo EM, Ren Y, Anaya-Eugenio GD, Ninh TN, Rakotondraibe HL, de Blanco EJC, Soejarto DD, Kinghorn AD. 2021. Spermidine alkaloid and glycosidic constituents of vietnamese *Homalium cochinchinensis*. *Phytochemistry Letters* **43**:154–162 DOI 10.1016/j.phytol.2021.04.002.

An F, Liu W, Wei X, Pan Z, Lu Y. 2018. Curdepsidone A, a depsidone from the marine-derived endophytic fungus *curvularia* sp. IFB-Z10. *Natural Product Communications* **13(7)**:865–866 DOI 10.1177/1934578X1801300720.

Anh CV, Kwon J, Kang JS, Lee H, Heo C, Shin HJ. 2022. Antibacterial and cytotoxic phenolic polyketides from two marine-derived fungal strains of *Aspergillus unguis*. *Pharmaceuticals (Basel)* **15(1)**:74 DOI 10.3390/ph15010074.

Assefa ST, Yang E, Chae S, Song M, Lee J, Cho M, Jang S. 2019. Alpha glucosidase inhibitory activities of plants with focus on common vegetables. *Plants* **9(1)**:2 DOI 10.3390/plants9010002.

Bahar AA, Ren D. 2013. Antimicrobial peptides. *Pharmaceuticals* **6(12)**:1543–1575 DOI 10.3390/ph6121543.

Bai SZ, Yang LG, Bai L. 2021. Two new depsidones from parmelia saxatilis. *Chemistry of Natural Compounds* **57(1)**:63–65 DOI 10.1007/s10600-021-03283-4.

Bay MV, Nam PC, Quang DT, Mechler A, Hien NK, Hoa NT, Vo QV. 2020. Theoretical study on the antioxidant activity of natural depsidones. *ACS Omega* **5(14)**:7895–7902 DOI 10.1021/acsomega.9b04179.

Bui V, Duong T, Chavasiri W, Nguyen K, Huynh B. 2022. A new depsidone from the lichen usnea ceratina arch. *Natural Products Research* **36(9)**:2263–2269 DOI 10.1080/14786419.2020.1828405.

Burt SR, Harper JK, Cool LG. 2022. A new depsidone from the neotricone-rich chemotype of the lichenised fungus *Usnea fulvoreagens*. *Natural Product Research* Epub ahead of print 15 February 2022 DOI 10.1080/14786419.2022.2038594.

Cardile V, Graziano ACE, Avola R, Madrid A, Russo A. 2022. Physodic acid sensitizes LNCaP prostate cancer cells to TRAIL-induced apoptosis. *Toxicology in Vitro* **84**:105432 DOI 10.1016/j.tiv.2022.105432.

Carpentier C, Barbeau X, Azelmat J, Vaillancourt K, Grenier D, Lagüe P, Voyer N. 2018. Lobaric acid and pseudodepsidones inhibit NF-κB signaling pathway by activation of PPAR-γ. *Bioorganic & Medicinal Chemistry* **26(22)**:5845–5851 DOI 10.1016/j.bmc.2018.10.035.

Chen L, Deng H, Cui H, Fang J, Zuo Z, Deng J, Li Y, Wang X, Zhao L. 2018a. Inflammatory responses and inflammation-associated diseases in organs. *Oncotarget* **9(6)**:7204–7218 DOI 10.18632/oncotarget.23208.

Chen JE, Pedron S, Shyu P, Hu Y, Sarkaria JN, Harley BA. 2018b. Influence of hyaluronic acid transitions in tumor microenvironment on glioblastoma malignancy and invasive behavior. *Frontiers in Materials* **5**:39 DOI 10.3389/fmats.2018.00039.

Chen Y, Sun L, Yang H, Li Z, Liu J, Ai H, Wang G, Feng T. 2020. Depsidones and diaryl ethers from potato endophytic fungus *Boeremia exigua*. *Fitoterapia* **141**:104483 DOI 10.1016/j.fitote.2020.104483.

Devi AP, Duong T, Ferron S, Beniddir MA, Dinh M, Nguyen V, Mac D, Boustie J, Chavasiri W, Le Pogam P. 2020. Salazinic acid-derived depsidones and diphenylethers with α-glucosidase inhibitory activity from the lichen *Parmotrema dilatatum*. *Planta Medica* **86(16)**:1216–1224 DOI 10.1055/a-1203-0623.

Dhingra S, Rahman NAA, Peile E, Rahman M, Sartelli M, Hassali MA, Islam T, Islam S, Haque M. 2020. Microbial resistance movements: an overview of global public health threats posed by antimicrobial resistance, and how best to counter. *Frontiers in Public Health* **8**:535668 DOI 10.3389/fpubh.2020.535668.

Di Paolo M, Papi L, Gori F, Turillazzi E. 2019. Natural products in neurodegenerative diseases: a great promise but an ethical challenge. *International Journal of Molecular Sciences* **20(20)**:5170 DOI 10.3390/ijms20205170.

Ding Y, An F, Zhu X, Yu H, Hao L, Lu Y. 2019. Curdepsidones B-G, six depsidones with anti-inflammatory activities from the marine-derived fungus *Curvularia* sp. IFB-Z10. *Marine Drugs* **17(5)**:266 DOI 10.3390/md17050266.

Dongmo Zeukang R, Siwe-Noundou X, Tagatsing Fotsing M, Tabopda Kuiate T, Mbafor JT, Krause RW, Choudhary MI, Atchadé AdT. 2019. Cordidepsine is a potential new anti-HIV depsidone from *Cordia millenii*, baker. *Molecules* **24(17)**:3202 DOI 10.3390/molecules24173202.

Duong HT. 2019. Phenolic compounds from *Pamotrema dilatatum* growing in Lam Dong province. *Science and Technology Development Journal* **22(1)**:114–119 DOI 10.32508/stdj.v22i1.1010.

Duong T, Chavasiri W, Boustie J, Nguyen K. 2015. New meta-depsidones and diphenyl ethers from the lichen *Parmotrema tsavoense* (Krog & Swinscow) Krog & Swinscow, Parmeliaceae. *Tetrahedron* **71(52)**:9684–9691 DOI 10.1016/j.tet.2015.06.107.

Duong T, Le Pogam P, Tran T, Mac D, Dinh M, Sichaem J. 2020. A-glucosidase inhibitory depsidones from the lichen parmotrema tsavoense. *Planta Medica* **86(11)**:776–781 DOI 10.1055/a-1179-1050.

Fagnani L, Nazzicone L, Bellio P, Franceschini N, Tondi D, Verri A, Petricca S, Iorio R, Amicosante G, Perilli M, Celenza G. 2022. Protocetraric and salazinic acids as potential inhibitors of SARS-CoV-2 3CL protease: biochemical, cytotoxic, and computational characterization of depsidones as slow-binding inactivators. *Pharmaceuticals* **5(6)**:714 DOI 10.3390/ph15060714.

Fjell CD, Hiss JA, Hancock RE, Schneider G. 2012. Designing antimicrobial peptides: form follows function. *Nature Reviews Drug Discovery* **11(1)**:37–51 DOI 10.1038/nrd3591.

González-Teuber M, Kaltenpoth M, Boland W. 2014. Mutualistic ants as an indirect defence against leaf pathogens. *New Phytologist* **202(2)**:640–650 DOI 10.1111/nph.12664.

Guo Z, Zhu W, Zhao L, Chen Y, Li S, Cheng P, Ge H, Tan R, Jiao R. 2022. New antibacterial depsidones from an ant-derived fungus *Spiromastix* sp. MY-1. *Chinese Journal of Natural Medicines* **20(8)**:627–632 DOI 10.1016/S1875-5364(22)60170-5.

Hao L, Zhou D, Qin X, Zhang W, Yang R, Li J, Huang X. 2022. A new depsidone derivative from mangrove endophytic fungus *Aspergillus* sp. GXNU-A9. *Natural Product Research* **36(7)**:1878–1882 DOI 10.1080/14786419.2020.1809400.

Hartati S, Megawati M, Antika LD. 2022. Parvidepsidone, a novel depsidone from the barks of *Garcinia parvifolia* Miq. *Natural Product Sciences* **28(1)**:13–17.

He R, Wang Y, Yang B, Liu Z, Li D, Zou B, Huang Y. 2022. Structural characterization and assessment of anti-inflammatory activities of polyphenols and depsidone derivatives from *Melastoma malabathricum* subsp. normale. *Molecules* **27(5)**:1521 DOI 10.3390/molecules27051521.

Ibrahim SR, Mohamed GA, Al Haidari RA, El-Kholy AA, Zayed MF, Khayat MT. 2018. Biologically active fungal depsidones: chemistry, biosynthesis, structural characterization, and bioactivities. *Fitoterapia* **129**:317–365 DOI 10.1016/j.fitote.2018.04.012.

Ibrahim SR, Sirwi A, Eid BG, Mohamed SG, Mohamed GA. 2021. Fungal depsides—Naturally inspiring molecules: biosynthesis, structural characterization, and biological activities. *Metabolites* **11(10)**:683 DOI 10.3390/metabo11100683.

Isaka M, Yangchum A, Supothina S, Veeranondha S, Komwijit S, Phongpaichit S. 2019. Semisynthesis and antibacterial activities of nidulin derivatives. *Journal of Antibiotics* **72(3)**:181–184 DOI 10.1038/s41429-018-0133-0.

Ismed F, Putra HE, Arifa N, Putra DP. 2021. Phytochemical profiling and antibacterial activities of extracts from five species of Sumatran lichen genus *Stereocaulon*. *Jordan Journal of Pharmaceutical Sciences* **14(2)**:189–202.

Jacome-Galarza CE, Percin GI, Muller JT, Mass E, Lazarov T, Eitler J, Rauner M, Yadav VK, Crozet L, Bohm M. 2019. Developmental origin, functional maintenance and genetic rescue of osteoclasts. *Nature* **568(7753)**:541–545 DOI 10.1038/s41586-019-1105-7.

Jia C, Xue J, Li X, Li D, Li Z, Hua H. 2019. New depsidone and dichromone from the stems of *Garcinia paucinervis* with antiproliferative activity. *Journal of Natural Medicines* **73(1)**:278–282 DOI 10.1007/s11418-018-1247-1.

Jin Y, Ma Y, Xie W, Hou L, Xu H, Zhang K, Zhang L, Du Y. 2018. UHPLC-Q-TOF-MS/MS-oriented characteristic components dataset and multivariate statistical techniques for the holistic quality control of usnea. *RSC Advances* **8(28)**:15487–15500 DOI 10.1039/C8RA00081F.

Khameneh B, Iranshahy M, Soheili V, Fazly Bazzaz BS. 2019. Review on plant antimicrobials: a mechanistic viewpoint. *Antimicrobial Resistance & Infection Control* **8(1)**:1–28 DOI 10.1186/s13756-019-0559-6.

Kilian LS, Voran J, Frank D, Rangrez AY. 2021. RhoA: a dubious molecule in cardiac pathophysiology. *Journal of Biomedical Science* **28(1)**:1–21 DOI 10.1186/s12929-021-00730-w.

Koo MH, Shin M, Ju Kim M, Lee S, Eun So J, Hee Kim J, Hyuck Lee J, Suh S, Joung Youn U. 2022. Bioactive secondary metabolites isolated from the Antarctic lichen *Himantormia lugubris*. *Chemistry & Biodiversity* **19(10)**:e202200374 DOI 10.1002/cbdv.202200374.

Lage TC, Maciel TMS, Mota YC, Sisto F, Sabino JR, Santos JC, Figueiredo IM, Masia C, de Fátima Â, Fernandes SA, Modolo LV. 2018. In vitro inhibition of helicobacter pylori and interaction studies of lichen natural products with jack bean urease. *New Journal of Chemistry* **42(7)**:5356–5366 DOI 10.1039/C8NJ00072G.

Lannang AM, Sema DK, Tatsimo SJ, Tankeu VT, Tegha HF, Wansi JD, Shiono Y, Sewald N. 2018. A new depsidone derivative from the leaves of *Garcinia polyantha*. *Natural Product Research* **32(9)**:1033–1038 DOI 10.1080/14786419.2017.1378201.

Leal A, Rojas JL, Valencia-Islas NA, Castellanos L. 2018. New β-orcinol depsides from *Hypotrachyna caraccensis*, a lichen from the páramo ecosystem and their free radical scavenging activity. *Natural Product Research* **32(12)**:1375–1382 DOI 10.1080/14786419.2017.1346639.

Li C, Naren AP. 2010. CFTR chloride channel in the apical compartments: Spatiotemporal coupling to its interacting partners. *Integrative Biology* **2(4)**:161–177 DOI 10.1039/b924455g.

Liang Y, Zheng Y, Shen Y, Li Q, Lu Y, Ye S, Li X, Li D, Chen C, Zhu H, Zhang Y. 2022. Two new depsidones from the fungus *Lasiodiplodia pseudotheobromae*. *Tetrahedron Letters* **105**:154046 DOI 10.1016/j.tetlet.2022.154046.

Lorenzati B, Zucco C, Miglietta S, Lamberti F, Bruno G. 2010. Oral hypoglycemic drugs: pathophysiological basis of their mechanism of action. *Pharmaceuticals* **3(9)**:3005–30020 DOI 10.3390/ph3093005.

Mathioudaki A, Berzesta A, Kypriotakis Z, Skaltsa H, Heilmann J. 2018. Phenolic metabolites from Hypericum kelleri Bald., an endemic species of Crete (Greece). *Phytochemistry* **146**:1–7 DOI 10.1016/j.phytochem.2017.11.009.

Misra S, Heldin P, Hascall VC, Karamanos NK, Skandalis SS, Markwald RR, Ghatak S. 2011. Hyaluronan-CD44 interactions as potential targets for cancer therapy. *The FEBS Journal* **278(9)**:1429–1443 DOI 10.1111/j.1742-4658.2011.08071.x.

Morshed MT, Nguyen HT, Vuong D, Crombie A, Lacey E, Ogunniyi AD, Page SW, Trott DJ, Piggott AM. 2021. Semisynthesis and biological evaluation of a focused library of unguinol

derivatives as next-generation antibiotics. *Organic & Biomolecular Chemistry* **19(5)**:1022–1036 DOI 10.1039/D0OB02460K.

Morshed MT, Vuong D, Crombie A, Lacey AE, Karuso P, Lacey E, Piggott AM. 2018. Expanding antibiotic chemical space around the nidulin pharmacophore. *Organic & Biomolecular Chemistry* **16(16)**:3038–3051 DOI 10.1039/C8OB00545A.

Nakashima K, Tomida J, Kamiya T, Hirai T, Morita Y, Hara H, Kawamura Y, Adachi T, Inoue M. 2018. Diaporthols A and B: bioactive diphenyl ether derivatives from an endophytic fungus *Diaporthe* sp. *Tetrahedron Letters* **59(13)**:1212–1215 DOI 10.1016/j.tetlet.2018.02.032.

Nguyen V, Genta-Jouve G, Duong T, Beniddir MA, Gallard J, Ferron S, Boustie J, Mouray E, Grellier P, Chavasiri W. 2020. Eumitrins CE: structurally diverse xanthone dimers from the Vietnamese lichen *Usnea baileyi*. *Fitoterapia* **141**:104449 DOI 10.1016/j.fitote.2019.104449.

Nguyen TT, Nallapaty S, Rao GK, Koneru ST, Annam SS, Tatipamula VB. 2021. Evaluating the in vitro activity of depsidones from *Usnea subfloridana* Stirton as key enzymes involved in inflammation and gout. *Pharmaceutical Sciences* **27(2)**:291–296 DOI 10.34172/PS.2020.73.

Nguyen T, Nguyen T, Nguyen T, Nguyen H, Nguyen N, Mai D, Huynh B, Tran C, Duong T. 2022a. Parmosidone K, a new meta-depsidone from the lichen *Parmotrema tsavoense*. *Natural Products Research* **36(8)**:2037–2042 DOI 10.1080/14786419.2020.1844697.

Nguyen HT, Polimati H, Annam SS, Okello E, Thai QM, Vu TY, Tatipamula VB. 2022b. Lobaric acid prevents the adverse effects of tetramethrin on the estrous cycle of female albino Wistar rats. *PLOS ONE* **17(7)**:e0269983 DOI 10.1371/journal.pone.0269983.

Niu S, Liu D, Shao Z, Huang J, Fan A, Lin W. 2021a. Chlorinated metabolites with antibacterial activities from a deep-sea-derived *Spiromastix* fungus. *RSC Advances* **11(47)**:29661–29667 DOI 10.1039/d1ra05736g.

Niu S, Liu D, Shao Z, Liu J, Fan A, Lin W. 2021b. Chemical epigenetic manipulation triggers the production of sesquiterpenes from the deep-sea derived *Eutypella* fungus. *Phytochemistry* **192**:112978 DOI 10.1016/j.phytochem.2021.112978.

Nugraha AS, Dayli IR, Permata C, Firli LN, Widhi Pratama AN, Triatmoko B, Untari LF, Wongso H, Keller PA, Wangchuk P. 2022. Isolation of antibacterial depside constituents from Indonesian folious lichen, *Candelaria fibrosa*. *Journal of Biologically Active Products from Nature* **12(1)**:24–32 DOI 10.1080/22311866.2021.2021986.

Olivon F, Nothias L, Dumontet V, Retailleau P, Berger S, Ferry G, Cohen W, Pfeiffer B, Boutin JA, Scalbert E. 2018. Natural inhibitors of the RhoA-p115 complex from the bark of Meiogyne baillonii. *Journal of Natural Products* **81(7)**:1610–1618 DOI 10.1021/acs.jnatprod.8b00209.

Ouyang J, Mao Z, Guo H, Xie Y, Cui Z, Sun J, Wu H, Wen X, Wang J, Shan T. 2018. Mollicellins O-R, four new depsidones isolated from the endophytic fungus *Chaetomium* sp. eef-10. *Molecules* **23(12)**:3218 DOI 10.3390/molecules23123218.

Papierska K, Krajka-Kuźniak V, Paluszczak J, Kleszcz R, Skalski M, Studzińska-Sroka E, Baer-Dubowska W. 2021. Lichen-derived depsides and depsidones modulate the Nrf2, NF-κB and STAT3 signaling pathways in colorectal cancer cells. *Molecules* **26(16)**:4787 DOI 10.3390/molecules26164787.

Pavan Kumar P, Siva B, Anand A, Tiwari AK, Vekata Rao C, Boustie J, Suresh Babu K. 2020. Isolation, semi-synthesis, free-radicals scavenging, and advanced glycation end products formation inhibitory constituents from *Parmotrema tinctorum*. *Journal of Asian Natural Products Research* **22(10)**:976–988 DOI 10.1080/10286020.2019.1628024.

Phainuphong P, Rukachaisirikul V, Phongpaichit S, Sakayaroj J, Kanjanasirirat P, Borwornpinyo S, Akrimajirachoote N, Yimnual C, Muanprasat C. 2018. Depsides and

depsidones from the soil-derived fungus *Aspergillus unguis* PSU-RSPG204. *Tetrahedron* **74(39)**:5691–5699 DOI 10.1016/j.tet.2018.07.059.

Promgool T, Kanokmedhakul K, Leewijit T, Song J, Soytong K, Yahuafai J, Kudera T, Kokoska L, Kanokmedhakul S. 2022. Cytotoxic and antibacterial depsidones from the endophytic fungus *Chaetomium brasiliense* isolated from Thai rice. *Natural Product Research* **36(18)**:4605–4613 DOI 10.1080/14786419.2021.1999947.

Rukachaisirikul V, Chinpha S, Saetang P, Phongpaichit S, Jungsuttiwong S, Hadsadee S, Sakayaroj J, Preedanon S, Temkitthawon P, Ingkaninan K. 2019. Depsidones and a dihydroxanthenone from the endophytic fungi *Simplicillium lanosoniveum* (JFH beyma) zare & W. gams PSU-H168 and PSU-H261. *Fitoterapia* **138**:104286 DOI 10.1016/j.fitote.2019.104286.

Sadorn K, Saepua S, Bunbamrung N, Boonyuen N, Komwijit S, Rachtawee P, Pittayakhajonwut P. 2022. Diphenyl ethers and depsidones from the endophytic fungus *Aspergillus unguis* BCC54176. *Tetrahedron* **105**:132612 DOI 10.1016/j.tet.2021.132612.

Saetang P, Rukachaisirikul V, Phongpaichit S, Preedanon S, Sakayaroj J, Hadsadee S, Jungsuttiwong S. 2021. Antibacterial and antifungal polyketides from the fungus *Aspergillus unguis* PSU-MF16. *Journal of Natural Products* **84(5)**:1498–1506 DOI 10.1021/acs.jnatprod.0c01308.

Sanjaya A, Avidlyandi A, Adfa M, Ninomiya M, Koketsu M. 2020. A new depsidone from *Teloschistes flavicans* and the antileukemic activity. *Journal of Oleo Science* **69(12)**:1591–1595 DOI 10.5650/jos.ess20209.

Sedrpoushan A, Haghi H, Sohrabi M. 2022. A new secondary metabolite profiling of the lichen *Diploschistes diacapsis* using liquid chromatography electrospray ionization tandem mass spectrometry. *Inorganic Chemistry Communications* **145**:110006 DOI 10.1016/j.inoche.2022.110006.

Sepúlveda B, Cornejo A, Bárcenas-Pérez D, Cheel J, Areche C. 2022. Two new fumarprotocetraric acid lactones identified and characterized by UHPLC-PDA/ESI/ORBITRAP/MS/MS from the Antarctic lichen *Cladonia metacorallifera*. *Separations* **9(2)**:41 DOI 10.3390/separations9020041.

Shen B. 2015. A new golden age of natural products drug discovery. *Cell* **163(6)**:1297–1300 DOI 10.1016/j.cell.2015.11.031.

Shiono Y, Koseki T, Koyama H. 2018. A bioactive depsidone from *Lachnum virgineum* (Hyaloscyphaceae). *Natural Product Sciences* **24(2)**:79–81 DOI 10.20307/nps.2018.24.2.79.

Shukla I, Azmi L, Gupta SS, Upreti DK, Rao CV. 2019. Amelioration of anti-hepatotoxic effect by *Lichen rangiferinus* against alcohol induced liver damage in rats. *Journal of Ayurveda and Integrative Medicine* **10(3)**:171–177 DOI 10.1016/j.jaim.2017.08.007.

Singh G, Armaleo D, Dal Grande F, Schmitt I. 2021. Depside and depsidone synthesis in lichenized fungi comes into focus through a genome-wide comparison of the olivetoric acid and physodic acid chemotypes of *Pseudevernia furfuracea*. *Biomolecules* **11(10)**:1445 DOI 10.3390/biom11101445.

Stojanovic G, Stojanovic I, Smelcerovic A. 2012. Lichen depsidones as potential novel pharmacologically active compounds. *Mini-Reviews in Organic Chemistry* **9(2)**:178–184 DOI 10.2174/157019312800604689.

Studzińska-Sroka E, Majchrzak-Celińska A, Zalewski P, Szwajgier D, Baranowska-Wójcik E, Żarowski M, Plech T, Cielecka-Piontek J. 2021. Permeability of hypogymnia physodes extract Component—Physodic acid through the Blood-Brain barrier as an important argument for its anticancer and neuroprotective activity within the central nervous system. *Cancers* **13(7)**:1717 DOI 10.3390/cancers13071717.
Sureram S, Kesornpun C, Mahidol C, Ruchirawat S, Kittakoop P. 2013. Directed biosynthesis through biohalogenation of secondary metabolites of the marine-derived fungus Aspergillus unguis. *RSC Advances* **3(6)**:1781–1788 DOI 10.1039/C2RA23021F.

Tan Y, Deng W, Zhang Y, Ke M, Zou B, Luo X, Su J, Wang Y, Xu J, Nandakumar KS. 2020. A marine fungus-derived nitrobenzoyl sesquiterpenoid suppresses receptor activator of NF-κB ligand-induced osteoclastogenesis and inflammatory bone destruction. *British Journal of Pharmacology* **177(18)**:4242–4260 DOI 10.1111/bph.15179.

Tatipamula VB, Annam SS. 2022. Antimycobacterial activity of acetone extract and isolated metabolites from folklore medicinal lichen *Usnea laevis* Nyl. against drug-sensitive and multidrug-resistant tuberculosis strains. *Journal of Ethnopharmacology* **282**:114641 DOI 10.1016/j.jep.2021.114641.

Thuan NH, Polimati H, Alluri R, Tatipamula VB. 2022. Bioassay-guided isolation of antimycobacterial substances from the traditionally used lichen *Cladonia pyxidata* (L.) Hoffm. *3 Biotech* **12(4)**:95 DOI 10.1007/s13205-022-03159-6.

Umeokoli BO, Ebrahim W, El-Neketi M, Müller WE, Kalscheuer R, Lin W, Liu Z, Proksch P. 2019. A new depsidone derivative from mangrove sediment derived fungus *Lasiodiplodia theobromae. Natural Product Research* **33(15)**:2215–2222 DOI 10.1080/14786419.2018.1496430.

Ureña-Vacas I, González-Burgos E, Divakar PK, Gómez-Serranillos MP. 2022. Lichen depsidones with biological interest. *Planta Medica* **88(11)**:855–880 DOI 10.1055/a-1482-6381.

Van Nguyen K, Duong T, Nguyen KPP, Sangvichien E, Wonganan P, Chavasiri W. 2018. Chemical constituents of the lichen usnea baileyi (stirt.) zahlbr. *Tetrahedron Letters* **59(14)**:1348–1351 DOI 10.1016/j.tetlet.2018.02.007.

World Health Organization. 2021. Diabetes; c2021. *Available at* https://www.who.int/news-room/fact-sheets/detail/diabetes (accessed 23 April 2022).

Xu J, Zhou L, Venturi V, He Y, Kojima M, Sakakibari H, Höfte M, De Vleesschauwer D. 2015. Phytohormone-mediated interkingdom signaling shapes the outcome of rice-*Xanthomonas oryzae* pv. *oryzae* interactions. *BMC Plant Biology* **15(1)**:1–16 DOI 10.1186/s12870-014-0411-3.

Yang W, Bao H, Liu Y, Nie Y, Yang J, Hong P, Zhang Y. 2018. Depsidone derivatives and a cyclopeptide produced by marine fungus *Aspergillus unguis* under chemical induction and by its plasma induced mutant. *Molecules* **23(9)**:2245 DOI 10.3390/molecules23092245.

Yang L, Wang Z, Wang Y, Li R, Wang F, Wang K. 2019. Phenolic constituents with neuroprotective activities from Hypericum wightianum. *Phytochemistry* **165**:112049 DOI 10.1016/j.phytochem.2019.112049.

Zhang Y, Li Z, Huang B, Liu K, Peng S, Liu X, Gao C, Liu Y, Tan Y, Luo X. 2022. Anti-osteoclastogenic and antibacterial effects of chlorinated polyketides from the Beibu Gulf coral-derived fungus *Aspergillus unguis* GXIMD 02505. *Marine Drugs* **20(3)**:178 DOI 10.3390/md20030178.

Zhang L, Niaz SI, Wang Z, Zhu Y, Lin Y, Li J, Liu L. 2018. α-Glucosidase inhibitory and cytotoxic botryorhodines from mangrove endophytic fungus *Trichoderma* sp. 307. *Natural Product Research* **32(24)**:2887–2892 DOI 10.1080/14786419.2017.1385023.

Zhao C, Liu G, Liu X, Zhang L, Li L, Liu L. 2020. Pycnidiophorones A-D, four new cytochalasans from the wetland derived fungus *Pycnidiophora dispersa. RSC Advances* **10(66)**:40384–40390 DOI 10.1039/d0ra08072a.

Zhao H, Wu L, Yan G, Chen Y, Zhou M, Wu Y, Li Y. 2021a. Inflammation and tumor progression: signaling pathways and targeted intervention. *Signal Transduction and Targeted Therapy* **6(1)**:1–46 DOI 10.1038/s41392-021-00658-5.

Zhao P, Yang M, Zhu G, Zhao B, Wang H, Liu H, Wang X, Qi J, Yin X, Yu L, Meng Y, Li Z, Zhang L, Xia X. 2021b. Mollicellins S-U, three new depsidones from *Chaetomium brasiliense* SD-596 with anti-MRSA activities. *The Journal of Antibiotics (Tokyo)* **74(5)**:317–323 DOI 10.1038/s41429-020-00398-8.

Zheng Y, Ley SH, Hu FB. 2018. Global aetiology and epidemiology of type 2 diabetes mellitus and its complications. *Nature Reviews Endocrinology* **14(2)**:88–98 DOI 10.1038/nrendo.2017.151.

Zwartsen A, Chottanapund S, Kittakoop P, Navasumrit P, Ruchirawat M, Van Duursen M, Van den Berg M. 2019. Evaluation of anti-tumour properties of two depsidones-Unguinol and Aspergillusidone D-in triple-negative MDA-MB-231 breast tumour cells. *Toxicology Reports* **6**:1216–1222 DOI 10.1016/j.toxrep.2019.10.012.